Ultrawideband Systems and Networks: Beyond $C + L$-Band

By Takeshi Hoshida, *Senior Member IEEE*, Vittorio Curri, *Senior Member IEEE*, Lidia Galdino, *Senior Member IEEE*, David T. Neilson, *Fellow IEEE*, Wladek Forysiak, *Member IEEE*, Johannes K. Fischer, *Senior Member IEEE*, Tomoyuki Kato, *Member IEEE*, and Pierluigi Poggiolini, *Fellow IEEE*

ABSTRACT | In the evolution of optical networks, spectral efficiency (SE) enhancement has been the most cost-efficient and thus the main driver for capacity increase for decades. As a result, the development of optical transport systems has been focused on the C- and L-bands, where silica optical fiber exhibits the lowest attenuation, and erbium-doped fiber amplifiers provide an efficient solution to compensate for the optical loss. With a gradual maturity in the SE growth, however, the extension of the optical bandwidth beyond the C + L-band is expected to play a significant role in future capacity upgrades of optical networks and, thus, attract increasing research interests. In this article, we discuss the merits and challenges of ultrawideband optical transport systems and networks beyond conventional bands.

KEYWORDS | Optical communication; optical network and switching; optical transceiver (TRx); Raman amplification; ultrawideband (UWB) transmission; wavelength conversion; wavelength-division multiplexing (WDM).

Manuscript received 30 September 2021; revised 22 April 2022; accepted 7 August 2022. The work of Vittorio Curri, Johannes K. Fischer, and Wladek Forysiak was supported by the EU Horizon 2020 under Grant 814276. The work of Lidia Galdino was supported by the Royal Academy of Engineering and EPSRC Program under Grant EP/R035342/1. The work of Pierluigi Poggiolini was supported by the PhotoNext Inter-Department Laboratory of Politecnico di Torino. *(Corresponding author: Takeshi Hoshida.)*

Takeshi Hoshida and **Tomoyuki Kato** are with Fujitsu Ltd., Kawasaki 211-8588, Japan (e-mail: hoshida@fujitsu.com; kato.tom@fujitsu.com).

Vittorio Curri and **Pierluigi Poggiolini** are with the Department of Electronics and Telecommunications, Politecnico di Torino, 10129 Turin, Italy (e-mail: vittorio.curri@polito.it; pierluigi.poggiolini@polito.it).

Lidia Galdino was with the Department of Electronic and Electrical Engineering, University College London, WC1E7JE London, U.K. She is now with Corning Optical Communications, CH5 3XD Ewloe, U.K. (e-mail: galdinol@corning.com).

David T. Neilson is with Nokia Bell Labs, Murray Hill, NJ 07974 USA (e-mail: david.neilson@nokia-bell-labs.com).

Wladek Forysiak is with the Department of Electrical and Electronic Engineering, Aston University, B4 7ET Birmingham, U.K. (e-mail: w.forysiak@aston.ac.uk).

Johannes K. Fischer is with the Fraunhofer Institute for Telecommunications, Heinrich Hertz Institute, 10587 Berlin, Germany (e-mail: johannes.fischer@hhi.fraunhofer.de).

Digital Object Identifier 10.1109/JPROC.2022.3202103

I. Introduction

Continuous efforts to enhance optical transport networks have resulted in a consistent increase in per-fiber capacity exceeding five orders of magnitude over four decades [1]. In core networks, the low-loss wavelength window of a silica-based optical fiber, as shown in Fig. 1, started to be exploited in the 1990s when wavelength-division multiplexing (WDM) technology around the 1550-nm wavelength was deployed along with the erbium-doped fiber amplifier (EDFA) [2], [3], [4].

By using gain flattening filters, it was possible to extend the useful frequency range of the EDFA to over 4 THz, and the first WDM band ranging from 1530 to 1565 nm, according to Supplement G.sup39 by the Telecommunication Standardization Sector of International Telecommunication Union (ITU-T) [5], was named the conventional band or C-band, which also corresponds to the minimum loss in a silica fiber. This was quickly followed by the commercialization of the long wavelength band or L-band, ranging from 1565 to 1625 nm, in the early 2000s. This was partly to double the number of WDM channels supported by a fiber strand but was also to deploy WDM systems on dispersion-shifted fiber infrastructures that are known to induce severe crosstalk due to the four-wave mixing (FWM) among WDM channels in the C-band running on the same fiber, especially in direct detection [6], [7]. Research toward further exploitation of the low-loss spectral window followed, including the S-band (ranging from 1460 to 1530 nm), the E-band (ranging from 1360 to 1460 nm), the O-band (ranging from 1260 to 1360 nm), and the U-band (ranging from 1625 to 1675 nm) [8], [9], [10], [11], [12], [13]. The definition of bands by ITU-T Supplement G.sup 39 is summarized in Table I.

However, these efforts have not resulted in immediate deployment because they have not been found to be

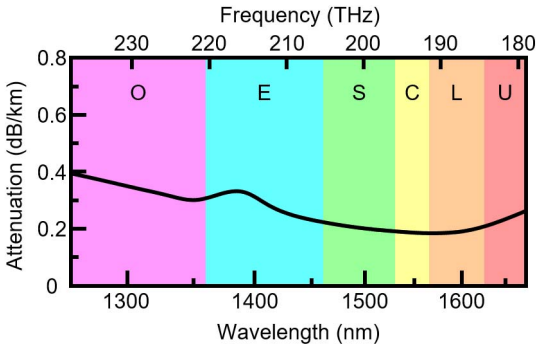

Fig. 1. *Low-loss window of the transmission fiber specified in ITU-T G.652. The horizontal axis is linearly scaled in frequency. Letters indicate band labels.*

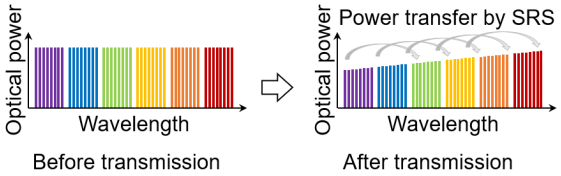

Fig. 2. *Schematic of changes in the optical spectrum due to SRS in fiber without wavelength-dependent loss.*

more efficient compared with the other means to increase capacity: dramatic enhancement of spectral efficiency (SE) was enabled by the invention of digital coherent transceivers (TRxs) in the late 2000s, i.e., denser WDM with narrower channel spacing and higher order modulation formats that carry more bits per symbol than previously deployed in 10-Gb/s direct detection systems. After more than a decade of continuous sophistication in digital coherent transceiver technology, however, the improvement of SE finally started to show a gradual slowdown of its pace as it approaches the Shannon capacity [14]. The extension of the wavelength band is, thus, becoming attractive again and resulted in efforts to extend the bandwidth of the amplifiers for C-band [15] and L-band systems [16], the deployment of numerous $C + L$-band systems [17], [18], [19], and the investigation of ultrawideband (UWB) systems[1] beyond the $C + L$-band by various organizations.

Challenges toward the development of practical UWB systems reside in several aspects. The first and simplest issue is the wavelength dependence of fiber parameters, such as loss, chromatic dispersion, and effective area, which could be approximated as constants in conventional systems. In addition, nonlinear interaction among WDM channels due to FWM, cross-phase modulation, and stimulated Raman scattering (SRS) in a transmission fiber impacts the channel characteristics [20], [21], [22], [23], [24]. SRS is particularly important in the context of a UWB transmission. Optical signals at the shorter wavelength (higher frequency) side of the spectrum are affected by the power transfer to the ones at the longer wavelength (lower frequency) side, resulting in the optical signal power of each channel deviating within the UWB signal spectrum considerably (see Fig. 2). A possible alternative to single-mode fibers (SMFs) for future UWB systems is hollow-core fibers (HCFs), in particular, the nested antiresonant nodeless fiber (NANF) [25]. Such fibers might provide a very wide bandwidth (300–400 nm) with attenuation comparable to SMF in the C-band [26], together with low dispersion and very low nonlinearity, including SRS. However, this is a very new technology that still needs substantial development to prove commercial viability. In addition, it requires the deployment of completely new cable infrastructure.

The remainder of this article starts with a discussion on the modeling of a UWB system, including such peculiarities in Section II. Then, we review the state of the art of UWB system demonstrations and their enabling techniques in Section III. Section IV discusses the implications of UWB systems in optical networking and node configuration, which is followed by related enabling technologies, such as optical switching, optical amplification, mitigation of UWB transceiver impairments, whole band wavelength conversion, and transmission in HCF.

[1]Many publications alternatively use the term multiband systems instead. In this contribution, we use the term UWB systems synonymously.

Table 1 Band Definition

Band	Wavelength range	Bandwidth in frequency
O	1260–1360 nm	17.5 THz
E	1360–1460 nm	15.1 THz
S	1460–1530 nm	9.4 THz
C	1530–1565 nm	4.4 THz
L	1565–1625 nm	7.1 THz
U	1625–1675 nm	5.5 THz

II. MODELING OF UWB TRANSMISSION SYSTEM

In this section, we address the peculiarities in modeling a multispan WDM optical fiber transmission over a bandwidth exceeding the state-of-the-art C-band and exploiting dual-polarization multilevel modulation formats with a digital signal processing (DSP)-based adaptive receiver—the so-called coherent optical technologies. The effect of WDM fiber propagation on such transmission technologies has been extensively analyzed in recent years, and several mathematical models of the physical effects have been proposed and validated. All derivations apply a perturbative approach and aim at describing the nature of the residual impairments after the equalized coherent receiver [27], [28]. These mathematical models can be subdivided into two main families: 1) models aiming at the evaluation of the worst case effect independently induced by each fiber span and modulation format agnostic: disaggregated

models, such as the incoherent GN model [29] and 2) those targeting the entire optically amplified line considering spatial transients and modulation format dependence: aggregated models, such as those of [30] and [31] and their evolutions. Models 1) are used in the planning and control of dynamic transparent networks where a disaggregated approach is needed [32], while models 2) enable to optimize point-to-point optical links in both long-haul and short-reach scenarios, for instance, in submarine cables and interdata-center connections. Independently of the specific approach, all theoretical derivations show that the effect of WDM fiber propagation can be summarized by introducing a disturbance caused by the nonlinear Kerr effect interacting with the chromatic dispersion and attenuation: the nonlinear interference (NLI). Such a disturbance, considered after the full chromatic dispersion compensation applied by the adaptive receiver together with the matched filter and the carrier phase recovery, at the optimal sampling time, has been extensively demonstrated to be well characterized as a dual-polarization additive Gaussian random process. In addition to the NLI, the other disturbance introduced by an optical line is the accumulated amplified spontaneous emission (ASE) noise from the optical amplifiers, which is well modeled as an additive dual-polarization Gaussian random process. Consequently, every transparent lightpath (LP) can be effectively modeled as a dual-polarization additive white and Gaussian noise (AWGN) nonlinear channel [33] characterized by its signal-to-noise ratio (SNR) [34], [35], [36]. Because of the presence of NLI, the LP SNR is typically defined as *generalized* optical SNR (GNSR) and is defined for the ith WDM channel as

$$\text{GSNR}_i = \frac{P_i}{P_{\text{ASE},i} + P_{\text{NLI},i}} \tag{1}$$

where P_i is the received channel power and $P_{\text{ASE},i}$ and $P_{\text{NLI},i}$ are the accumulated ASE noise and NLI, evaluated over a bandwidth equal to the symbol rate (R_s), respectively [35]. As the LP is a nonlinear channel, its GSNR can be maximized by properly setting the power per channel at the input of fiber spans [37]. The AWGN model for LPs has been extensively proven to be accurate, also in commercial scenarios, using different modulation formats and on mixed fiber types with a chromatic dispersion down to 2 ps/nm/km, using state-of-the-art symbol rates, or larger [34], [38]. This approach allows to apply the Shannon theory [14] to the WDM optical transmission, so the capacity limit of a WDM comb over an amplified fiber link can be defined as

$$C = 2\sum_{i=1}^{N_{\text{ch}}} R_{s,i}\log_2\left(1+\text{GSNR}_i\right) \quad \left[\frac{\text{bit}}{\text{sec}}\right] \tag{2}$$

where the factor 2 accounts for the dual-polarization and $R_{s,i}$ and GSNR_i are the symbol rate and GSNR for the ith WDM channel, respectively. To better show the need for additional spectrum to enlarge the link capacity, it is useful to focus on the simplified scenario of a fixed WDM grid Δf and a uniform symbol rate R_s together with a flat GSNR. Therefore, (2) is simplified to $C = 2\ B\ (R_s/\Delta f)\ \log_2(1+\text{GSNR})$, where $B = N_{\text{ch}}\Delta f$ is the total transmission bandwidth. State-of-the-art transceivers are very close to the limit [39], thanks to $R_s/\Delta f$ approaching the unit (e.g., $R_s = 69$ GBd in $\Delta f = 75$ GHz), the rate flexibility enabled by hybrid formats [40], and shaped constellations [41]. Some further capacity can be obtained by using hybrid EDFA/distributed Raman amplification [42] and/or using DSP techniques to partially compensate for the NLI [43], which increases the optimal GSNR, but the effect on the capacity of larger GSNR levels is limited by the logarithmic law. Therefore, to obtain more capacity, the total transmission bandwidth B must be enlarged, either by activating a new fiber line or exploiting additional bands on the same fiber line, as proposed in this work.

The available mathematical models for the NLI generation can be extended to their use on the UWB transmission from the O-band to the U-band, with the exception of a guard band around the zero-dispersion wavelength that is in the O-band for standard SMF (SSMF). The requested guard bandwidth depends on the minimum tolerable chromatic dispersion by the transmission technique, channel spacing, and power levels used in the spectral region. Moreover, the statistics of the zero-dispersion wavelength that may vary fiber by fiber are relevant in defining the guard band. At the end of this section, we will comment on the modeling transmission close to the zero-dispersion wavelength.

In UWB scenarios, the wave equation governing the evolution of the modal amplitude in the SMF is the same coupled nonlinear Schrödinger equation (CNLSE) as that for the C-band analysis because the fiber is in the single-mode regime, and nonlinearities are perturbations on the entire O-to-U-band spectrum [20]. Note that, in general, the CNLSE is a stochastic equation, as it includes the random birefringence. Focusing on the analysis of propagation of dual-polarization coherent optical technologies, the propagating optical signal is depolarized over short propagation distances, so we can apply a polarization average to the wave equation. Moreover, polarization mode dispersion (PMD) is typically compensated for by adaptive coherent receivers and weakly interacts with NLI generation. Consequently, we can assume the fiber wave equation to be the Manakov equation [44] centered at the wavelength of the channel under test. The WDM spectrum is the comb of the dual-polarization spectrally orthogonal N_{ch}, which are statistically independent random processes. Substituting such a signal form in the Manakov equation, we obtain a set of N_{ch} wave equations, each including loss, chromatic dispersion, and self- and cross-channel nonlinear effects: the spectrally separated Manakov equation (SSME). Nonlinear effects are always a perturbation, so each channel is assumed to propagate in accordance

with the following perturbative law:

$$\bar{A}_i(f,z) = \left\{\bar{A}_i(f,0) + \bar{N}_i(f,z)\right\}\sqrt{p_i(z)}H_{D,i}(f,z) \quad (3)$$

where f is the frequency and z is the propagation distance. $\bar{A}_i(f,z) = [A_{x,i}, A_{y,i}]^T$ is the optical field amplitude of the ith channel under test, $p_i(z)$ is the power evolution including loss and SRS [23], [24] effects, $H_{D,i}(f,z)$ is the effect of chromatic dispersion, and $\bar{N}_i(f,z) = [N_{x,i}, N_{y,i}]^T$ is the NLI spectrally centered on the ith channel. Substituting (3) in the SSME, the set of differential equations is obtained for the generation of the N_{ch} $\bar{N}_i(f,z)$ components. Integrating the equations and relying on the statistical properties of digital signals, the power spectral density $G_{N,i}(f)$ of $\bar{N}_i(f,z)$ can be evaluated. The coherent receiver applies the matched filter, so the intensity of the NLI Gaussian random process impairing the decision signal is $P_{\text{NLI},i} = \int_{-\infty}^{+\infty} G_{N,i}(f)|H_m(f)|^2 \mathrm{d}f$. Different mathematical models proposed in the literature rely on different approaches and approximations for the $P_{\text{NLI},i}$ calculation, but all can be summarized in the following common form:

$$P_{\text{NLI},i} = \eta_{\text{SPM},i}P_i^3 + P_i\sum_{j\neq i}\eta_{\text{XPM},ij}P_j^2 + \sum_{\text{klm}\in\text{FWM}_i}\eta_{\text{FWM,iklm}}P_kP_lP_m \quad (4)$$

where P_i is the input power of the ith channel, FWM_i is the set of FWM indices klm on the ith channel, and $\eta_{\text{SPM},i}$, $\eta_{\text{XPM},i}$, and $\eta_{\text{FWM,iklm}}$ are the efficiencies for self- and cross-phase modulations, and FWM, respectively, which generate the self-, cross-, and multichannel NLI components, respectively. For most practical scenarios, FWM is negligible, so the NLI components can be spectrally separated. Aggregated mathematical models focus on computing the overall NLI generated by the optical link by integrating the differential equation for $N_i(f,z)$ on the entire transmission system, while the disaggregated NLI models aim at the evaluation of the equivalent NLI generated by each fiber span.

In UWB scenarios, contrary to the C-band analyses, typical approximations in fiber parameters must be removed to properly take into account frequency dependencies across the wide bandwidth, starting with variations in the frequency of loss and chromatic dispersion [20]. The Kerr effect can still be considered as instantaneous [45], while scaling with the wavelength λ of the channel under test in the effective area, and consequently that of the nonlinear coefficient γ, must be included [20].

Specifically, variations with f of loss must be accurately considered. An effective method to properly consider variations with f of loss is to rely on the phenomenological expansion proposed in [46]

$$\alpha(\lambda) \simeq \alpha_S(\lambda) + \alpha_{\text{UV}}(\lambda) + \alpha_{\text{IR}}(\lambda) + \alpha_{13}(\lambda) \quad (5)$$

where $\alpha_S(\lambda), \alpha_{\text{UV}}(\lambda), \alpha_{\text{IR}}(\lambda)$, and $\alpha_{13}(\lambda)$ are the Rayleigh scattering, ultraviolet, infrared, and OH^- peak absorption contributions, respectively. In [47], it has been experimentally shown as this phenomenological approach is effective and needs to define only four parameters for an accurate and reliable loss profile model.

The SRS has a negligible effect on the modulation time constant [48], so its practical impairment on WDM signal combs is a seamless transfer of optical power from higher to lower frequencies depending on the frequency spacing Δf, with the efficiency peak of Δf around 12 THz [49], [50]. This means that the SRS can be considered a power-dependent spectral tilt for the C-band-only transmission, while, in the case when the fiber spectral exploitation approaches or exceeds 12 THz, the effect of SRS on per-channel power evolution must be accurately evaluated [51] given the power spectral density at the fiber input by solving the SRS set of N_{ch} differential equations [24], [52]

$$\frac{\partial P_n(z)}{\partial z} = -\alpha_n P_n(z) + -P_n(z)\sum_{m=1}^{n-1}C_R(f_n;\Delta f_{nm})P_m(z) + P_n(z)\sum_{m=n+1}^{N_{\text{ch}}}C_R(f_m;\Delta f_{mn})P_m(z) \quad (6)$$

where $P(z)$ is the power evolution of the nth channel centered at f_n in the N_{ch} WDM channel comb, α_n is the loss coefficient for the nth channel, $\Delta f_{nm} = f_n - f_m$, and $C_R(f_n;\Delta f_{nm})$ is the Raman efficiency referring to f_n for the spectral separation Δf_{nm}. Note that, to achieve an accurate evaluation of SRS, a proper shape for the Raman profile and its scaling with a reference frequency must be considered [49], [51].

Given the input power per channel $P_n = P_n(0)$, the solution of (6) is the per-channel power evolution $P_n(z) = P_n \cdot p_n(z) = P_n \exp(-\alpha_n z)G_{SRS,n}(z)$. To show the effect of SRS, as shown in Fig. 3, the UWB loss modified by the SRS over 70 km of the SSMF without OH^- absorption (ITU-T G.652D fiber) is depicted together with the intrinsic fiber loss. The full spectral load ($\Delta f = 75$ GHz and $R_s = 64$ GBd) from the O-band to the U-band is considered, and the input power per channel has been optimized to maximize the GSNR without considering the effect of SRS. A simple flat single-band power optimization on each per-band center channel [37] has been applied. To better focus on the effect of fiber, amplifiers are considered ideal with noise figures (NFs) [19] of 7 dB for the S- and O-bands, 6 dB for the E-, L-, and U-bands, and 5.5 dB for the C-band. Using these hypotheses, (6) has been solved on the O-to-U-band, considering the loss $\alpha(f_n)$ and Raman $C_R(f_n;\Delta f_{nm})$ profiles of the SSMF, including the Raman efficiency scaling with f_n [49]. Results are shown in Fig. 3, where it can be observed that all higher

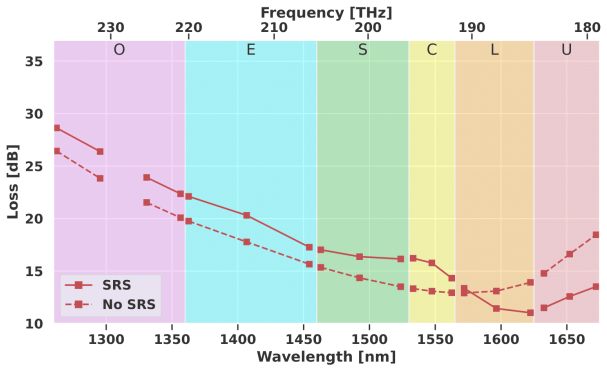

Fig. 3. ***Loss introduced by 70 km of the SSMF: fiber loss only (dashed) and fiber loss, including the SRS effect (solid). Flat per-band input power per channel optimized without SRS.***

frequencies for which the overall spectrally occupied lower frequencies exceed the Raman peak—roughly the O- to S-band—experience an extra loss due to SRS *depletion*. In contrast, with a change of regime in the C-band, frequencies without an occupied spectrum exceeding the SRS peak at lower frequencies experience a loss reduction due to SRS enhancement. Therefore, the SRS is the main UWB effect that, depending on the overall spectral load, enlarges loss at larger frequencies, enhancing the ASE noise impairments and reducing the NLI. The opposite occurs for lower frequencies, for which the SRS enhancement mitigates loss, therefore reducing the effect of ASE noise and enhancing the NLI generation. These UWB effects must be accurately considered in the mathematical NLI models when applied to UWB scenarios; otherwise, they rapidly lose accuracy with the expansion of spectral occupation beyond the C-band. Thus, mathematical models for the NLI generations must be adjusted by including the per-channel power profile $P_n(z)$ obtained by solving the SRS equations (6). For instance, the generalization of the GN model by including the SRS and loss profile has been proposed and validated in [36], [53], and [54].

To observe the impact of the UWB loss profile and that of SRS, in Fig. 4, we display the GSNR and its optical SNR (OSNR) and SNR_{NL} components evaluated [36] on the 70-km scenario considered for the loss plots of Fig. 3. These results have been obtained considering typical SSMF chromatic dispersion and loss profiles with respect to the frequency [19]. The fiber effective area is supposed 80 μm^2 in the C-band scaling with the inverse of the frequency in the other bands [49]. As expected, if we do not include the SRS (dotted-dashed curves), the OSNR component is always 3 dB lower than the SNR_{NL} at each band center frequency. The scenario drastically mutates when properly considering the SRS in evaluating the GSNR and its components. By analyzing these results shown in Fig. 4 (dotted curves), it is evident how the SRS depletion impacts O-to-S-bands by reducing the OSNR and enlarging the SNR_{NL}. This trend is consistent with the results in [19, Fig. 8], while quantitative difference appears due to different assumptions on the fiber parameters, as well as different baud rates and channel spacings, and different strategies to optimize fiber launch power. In [19], the considered larger power spectral density emphasizes the high- versus low-frequency regimes. Therefore, these bands operate in almost a linear regime with the GSNR defined by the OSNR—SNR_{NL} practically negligible—and reduced by 1–2 dB with respect to the prediction without considering the SRS. The opposite occurs for the L- and U-bands that are forced to operate in the nonlinear regime. For these bands, the GSNR is not reduced because of the strong benefits in the OSNR due to SRS enhancement that compensates for the SNR_{NL} reduction. The C-band is the transition from one regime to the other. Practical implications of this behavior are given as follows: 1) to properly manage UWB optical transport, the GSNR computation must accurately include the effect of SRS in both OSNR and SNR_{NL} computations; 2) the optical controller setting the amplifiers, and consequently the fiber input power per channel for each band, must be an MB optical controller that sets all the per-band amplifiers [55]; and 3) deploying traffic on additional bands on the same fiber must be accurately controlled to avoid GSNR reduction and, as a result, the possibility of service outages on already active WDM channels.

Finally, we comment on modeling fiber transmission when approaching the zero-dispersion wavelength λ_{zd}. When the chromatic dispersion approaches zero, the nature of the problem is modified, the perturbative approach must be modified as proposed in [56], and relevant parametric phenomena may impact propagation [20]. Moreover, in such a spectral region, considering the statistical variations of λ_{zd} in cables [57] becomes crucial because of possible chromatic dispersion magnitude variations being comparable with its nominal value. Thus, a clear assessment of nonlinear transmission modeling in such a spectral region has not yet been proposed. From a

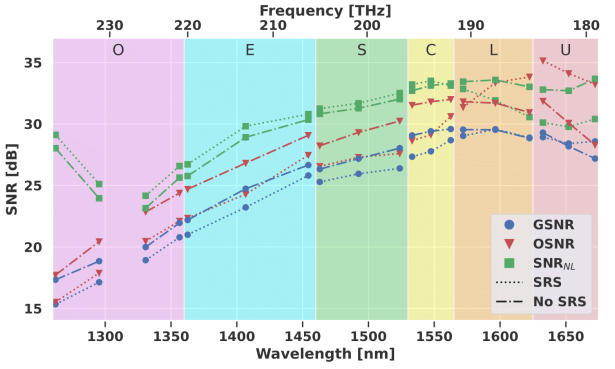

Fig. 4. ***GSNR (blue) with and without the SRS effect, together with OSNR (red) and SNR_{NL} (green) components, by 70 km of the SSMF. Flat per-band input power per channel optimized without SRS.***

practical perspective, the stochastic nature of the problem, and consequent possible issues on reliable LP deployment, suggests exploiting the spectral region around the nominal λ_{zd} for short-reach transmission only with the power level kept below the nonlinear threshold.

III. EXPERIMENTAL DEMONSTRATIONS OF UWB TRANSMISSION AND ENABLING TECHNIQUES

Research in SMF communication systems is currently being driven by two complementary strategies: bandwidth expansion and SE enhancement. It is, therefore, unsurprising that high-capacity SMF transmission system demonstrations regularly showcase new communications technologies while providing a key indicator of progress in the field as a whole. Several milestones in the achievable data throughput in SMF [58], [59], [60], [61], [62], [63], [64], [65], [66], [67], [68], [69] reported over the past decade are shown in Fig. 5. Particularly, it highlights the different amplification technologies that enabled the transmission bandwidth beyond the conventional $C + L$-band. Few efforts have been made to maximize capacity through transmission bandwidth extension in trans-Atlantic (>6000 km) and trans-Pacific (>9000 km) systems. These transmission systems are electrical power feed constrained, and optical fiber parallelism is seen as a better solution to maximize cable capacity. In contrast, record capacities over short transmission distances have mainly used amplification technologies that extend bandwidth beyond $C + L$-band EDFAs. In [61], a semiconductor optical amplifier (SOA) with a 100-nm gain bandwidth demonstrated the potential for an SMF capacity of 115.9 Tbit/s over a 100-km transmission distance. The relatively high NF of SOAs versus, for example, EDFAs, means that they are generally considered unsuitable for repeatered transmission systems. Nevertheless, by combining an SOA with distributed backward Raman amplification, a 107-Tbit/s transmission over 300 km (3×100 km) was reported in [63]. In [62], a distributed Raman amplifier with a 11.2-THz bandwidth enabled a 102-Tbit/s transmission over 240 km (3×80 km). An even greater data rate of 120 Tbit/s over 630 km (9×70 km) was shown by using hybrid distributed Raman-EDFA amplifiers with a continuous 91-nm gain bandwidth [64]. Further extension in transmission bandwidth toward lower S-band wavelengths resulted in a higher SMF capacity. In [60], a 150.3-Tbit/s transmission over 40 km was demonstrated. The transmitted signals occupied a total bandwidth of approximately 109 nm (13.625 THz), and a distributed backward Raman amplification scheme for the S-band and EDFAs for the C- and L-bands were used to compensate for the fiber loss. In [59], the combination of a thulium-doped fiber amplifier (TDFA), discrete Raman amplifiers, and $C + L$-band EDFAs provided a continuous gain bandwidth of 16.83 THz (1484.86–1619.67 nm), achieving a net throughput of 178.08 Tbit/s over 40 km. In [58], a record net data throughput of 190 Tbit/s over 54 km was shown. The channels were transmitted over a gain bandwidth of approximately 17.25 THz, and a hybrid distributed Raman/TDFA for S-band, together with $C + L$-band EDFAs, was used for signal amplification. Fig. 5 summarizes the transmission performance achievable with state-of-the-art technology under specific conditions. In the design of commercial systems, it is necessary to ensure dynamic range and margin to cope with variations in various parameters, such as span loss and aging of components. It is, therefore, appropriate to understand that these hero experiments are somewhat beyond the upper limits of performance achievable with commercial systems.

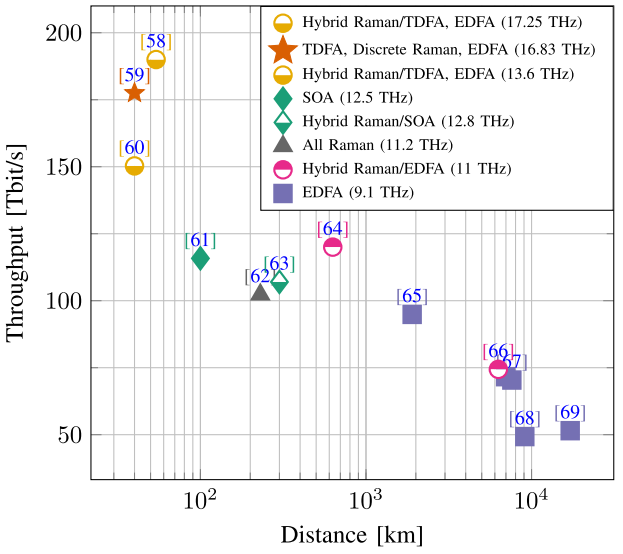

Fig. 5. ***Record data throughput versus distance for single-mode fiber. The transmission bandwidth indicated in each case is for the usable spectrum, not including spectral gaps between amplifier gain bandwidths.***

A UWB transmission architecture has already been envisioned in [70]. Even though UWB components are still unavailable, powerful experimental laboratory techniques, which permitted savings and massive duplication of equipment, have enabled the experimental demonstration of large-scale WDM systems [1]. For wideband transmissions, different lab approaches to emulate the aggressors' channels per band have been demonstrated. In [60], 47 carrier signals from DFB-LD and an I/Q subcarrier generator were used to generate 84 carrier signals. In [58], a single wideband comb source generated the interfering carriers across the entire 17.25-THz transmission bandwidth, and a single IQ-modulator was used to modulate all carriers. However, the spectral region of S-band wavelengths of the comb had a lower optical power, which contributed to worse channel performance at this band. To overcome this lower optical power per comb line at S-band wavelengths in [71], the same wideband comb source was used by Puttnam *et al.* to generate the carriers over only the C- and L-bands, and a single modulator was used to modulate the interfering channels in the $C + L$-bands. The S-band interfering

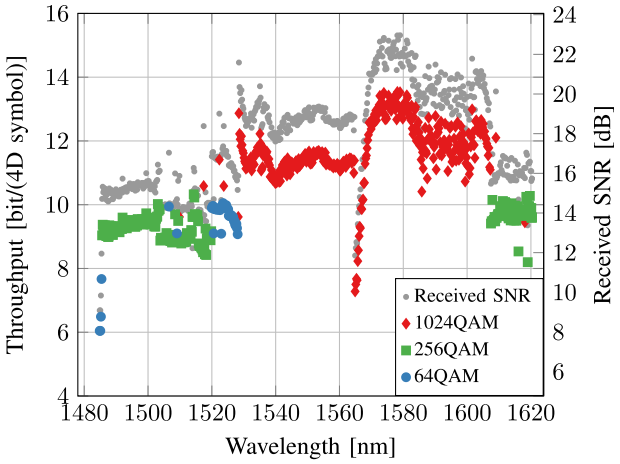

Fig. 6. ***Per-channel throughput and SNR over two polarizations after 40 km.***

modulated channels were generated by band wavelength conversion from an amplified tap of the L-band modulated channels.

An even simpler technique used to emulate the aggressors' channels, which is valid for high-SE dispersion-unmanaged coherent systems, uses the ASE of optical amplifiers, whose Gaussian optical field statistics accurately emulates a tightly packed broadband multiplex of spectrally and constellation-shaped WDM channels [72], [73]. In [61] and [63], a combination of banks of lasers together with ASE noise sources were used to emulate a continuous 12.5-THz bandwidth aggressor channel, while continuous 11- and 16.8-THz ASE noise sources were used in [64], [66], and [59], respectively.

Another experimental test-bed architecture solution and commercial product alternative for UWB transmission is whole band wavelength conversion for signal generation and reception proposed in [74]. Details of this new approach are given in Section IV-D.

These laboratory schemes have enabled the experimental demonstration of up to a 17-THz occupied transmission bandwidth, achieved by simultaneously using the S-, C-, and L-bands. However, it is important to note that, to date, for all wideband experimental demonstrations [58], [59], [60], [61], [63], [74], the S-band channel wavelengths (<1530 nm) experienced worse received performance compared with the C- and L-band wavelengths. For instance, Fig. 6 illustrates the information rate and received SNR for all 660 channels at 25-GBd channels after a 40-km transmission (details of the transmission system under investigation can be found in [59]). In this particular system, the combination of fiber parameters, hybrid amplification method, and different back-to-back implementation penalties per band leads to a significant SNR wavelength dependence (details are given in Section IV-D and [75]). To mitigate this effect and maximize the achievable information rate (AIR) of each individual channel, new geometrically shaped (GS) constellations tailored for the SNR of each wavelength were designed and implemented [59]. As can be seen in Fig. 6, in the C- and L-bands, 1024-*ary* GS constellations were mainly used, while, for channel wavelengths <1530 nm, GS-64-QAM and GS-256-QAM provided higher AIRs.

To date, only approximately a third of the low-loss window of a single-mode silica fiber bandwidth has been experimentally demonstrated. Notwithstanding seamless amplification technology can be designed and developed, experimentally study a fully-ed 50-THz SMF transmission system in a simplified and inexpensive manner remains a challenge. Due to the absence of seamless amplification technology, experimental study of fully loaded 50-THz SMF transmission system in a simplified and inexpensive manner remains a challenge.

IV. IMPLICATION OF UWB SYSTEM IN OPTICAL NETWORKING AND SWITCHING

When considering the suitability of UWB systems, we must consider the constraints placed on optical systems in different parts of the network. Transoceanic communication cables [76] have often been at the forefront of adopting fiber technologies, including EDFA [77]. Because these systems deploy both amplifiers and fiber at the same time, the issue of legacy fiber losses is less problematic. For repeated undersea systems, such as transoceanic cables, there is a constraint on total system power and the cross-sectional diameter of the cable. Therefore, increasing available optical bandwidth looks to be a promising way to scale cable capacity if broader band optical amplifiers with high efficiency and low NFs can be developed. Expansion of the optical bandwidth can lead to lower power per bit per amplifier by enabling a reduction in the SE that results in a larger reduction in power. This is applicable to both UWB and space-division multiplexing approaches.

In terrestrial systems, the potential application space may be subject to a different set of constraints. It is likely that they will have to operate over an installed fiber, which may limit the available spectrum due to higher transmission losses in other bands, as shown in Fig. 1. In longer haul systems (typically greater than 500 km), the fiber span lengths (80–120 km) may cause certain fiber bands, such as O and E, to have unacceptably high losses, unless amplifier spacing were reduced. However, in the metro space, where low-latency 5G applications and video streaming may drive rapid growth in demand, fiber spans can be significantly shorter (10–40 km), and much larger fiber bandwidths may become an attractive way to scale capacity on existing fiber plants (see Fig. 7). Unlike in early WDM systems where maintaining constant noise performance across the wavelength range was critical for system capacity, today's coherent transponders enable the capacity to be adjusted on the basis of the noise and impairments of each particular channel. This somewhat alleviates the need for constant losses and NFs from each amplifier or band.

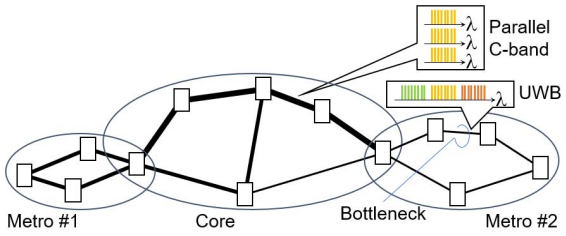

Fig. 7. ***Schematic for metro/core network based on UWB and conventional dense WDM. For segments with limited fiber availability (shown by thin lines), UWB transmission should be efficient in upgrading the network capacity without a new fiber deployment, while fiber-rich segments can use parallel conventional systems.***

To support the UWB network, it is necessary to expand the wavelength coverage of network elements, such as transceivers, in-line amplifiers, and switch nodes, such as the reconfigurable optical add-drop multiplexer (ROADM) or wavelength cross-connect. The actual node configuration that supports the UWB network should be designed in view of the limitations of practical optical components and subsystems. Fig. 8 shows one possible configurations for a three-degree ROADM node, having a transmission fiber in/out of three directions and local add/drop ports to be interfaced with transponders. In this example, the input/output interfaces to the transmission fibers are with wavelength-band multiplexers and demultiplexers so that different types of amplifiers and wavelength-selective switches (WSSs) are used in parallel to amplify and switch different portions of the UWB spectrum. The local add/drop port adopts a single UWB multicast switch (MCS) so that any transponder connected to any port can be routed from/to the appropriate WSS with the intended band and direction. Note that the node should become simpler if a single amplifier and/or a single WSS can handle multiple band signals together. In the following, several key technologies to support the future evolution of UWB networking are provided. For complementary and detailed discussions on the UWB devices and subsystems, the readers are also encouraged to look into another paper in this special issue [78].

A. Wavelength Switching

Current wavelength switching architecture [79] consists of using WSSs to build mesh-connected nodes with the option to add and drop local traffic. Internally, a WSS is an optical system that forms a spectrometer that disperses the light across a switching element, which is used to switch selected wavelengths to the needed output ports. The spectrometer is constructed using lenses, mirrors, gratings, and polarization optics, and the switching element is typically a liquid crystal on silicon (LCoS) reflective phase modulator, which is used to create holograms that steer portions of the spectrum to different ports. In current optical transport systems, a WSS typically covers either the C- or L-band and, typically, has 20 or more optical output ports to enable mesh connections, and so a $C + L$ system will typically have a band splitter and two WSSs per fiber. If this approach is used to open up additional spectral bands, as shown in Fig. 8, this introduces the same system switching complexity as using more fibers. The technologies for constructing WSSs can be adapted to operate in different wavelength bands [80] or over larger (36 THz) optical spectra [81] with the recent commercial implementation of 10 THz [82]. There are a number of constraints on the functionality as the switches are scaled to larger bandwidths. The spectral resolution of a WSS is limited by a combination of the spectrometer resolution, which is determined by the number of lines of the grating that is illuminated and by the number of pixels on the LCoS. Maintaining the same absolute spectral resolution while increasing the spectral width requires a larger number of pixels, leading to a larger LCoS panel or higher numerical aperture optics that will increase the overall system's size and cost. Alternatively, if the spectral resolution is scaled with the total spectral width, such that the system maintains the same number of resolvable spectral channels, the WSSs will have essentially the same footprint and complexity. The increased use of superchannels, where multiple transponders are combined into a single band, indicates that the need to maintain the spectral resolution to efficiently route a single transponder may not be necessary. If the current network topology is retained, maintaining the same number of channels is sufficient to enable the same connectivity as today, but at a higher per link capacity.

B. Amplification Technologies

Optical amplifiers were first used widely, instead of electronic repeaters, in optical transmission systems in the late

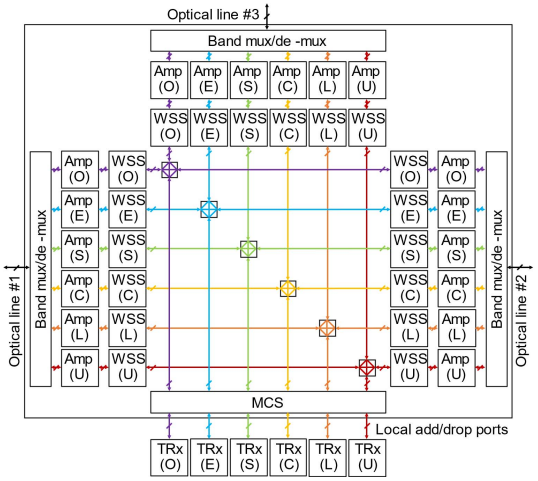

Fig. 8. ***Exemplified block diagram for UWB three-degree ROADM node having banded amplifiers, banded WSSs, and UWB MCS connected to banded transceivers.***

1990s, thanks to the invention of the EDFA. Although the C-band (in particular) and L-band EDFAs have undergone constant improvement, particularly in terms of functionality, size, and cost, their spectral coverage has remained limited to approximately 40 nm in each band. Alternative rare-earth-doped fiber amplifiers for the O-, E-, S-, and U-bands have yet to be developed to sufficient maturity levels for widespread adoption in commercial transmission systems [83]. Therefore, although rare-earth-doped fibers based on thulium (S-band), neodymium (E-band), and praseodymium (O-band) have been demonstrated in numerous experiments and are also available commercially [84], and bismuth-doped fiber amplifiers offer potential amplification windows over various parts of the UWB spectrum considered here [85], [86], there remain practical manufacturing, handling, and reliability issues yet to be solved. Similarly, long-standing alternative optical amplification technologies based on semiconductor optical amplifiers [87] and optical parametric amplifiers [88], [89] have significant associated challenges in terms of either introducing nonlinear distortions, or with power efficiency and compactness, for them to be deployed in practice, despite a number of attractive features, including the recently demonstrated 100-nm bandwidth [87] and low NF plus supplementary functionality [89], respectively. In terms of spectral flexibility for UWB transmission, the Raman amplifier offers a potential short-term solution to amplification in most of the target UWB spectrum because, as explained in the following, it can provide an arbitrary gain bandwidth, and the key components, high-power pump lasers, can be manufactured using existing, well-established techniques [83], [84].

The Raman amplification in optical fiber is a long-standing all-optical amplification technology whose promise was widely explored in the 1990s and was commercially deployed in the early 2000s [16], [90]. However, its development slowed in the late 2000s, as explained in Section I, due to the rapid increases in SE enabled by digital coherent transceivers [1]. Nevertheless, Raman amplifiers have found widespread commercial application over the years [52], [90], [91], both in long-distance, single-span, unrepeatered transmissions, where distributed, or even multiple-order, Raman amplification provides improved NF [92] but also in conventional long-haul systems [90], where the long-standing, occasional use of hybrid EDFA/distributed Raman amplification technologies [93] has become much more common recently to support the higher OSNR requirements of advanced modulation formats [94]. In the context of UWB systems and networks, the highly flexible spectral characteristics of Raman amplifiers, which are mainly determined by the availability of suitably high-power pump lasers of appropriate wavelength, offer the potential for MB or even seamless UWB Raman amplification, either when deployed in their own right, or in concert with established C-band, or $C + L$-band EDFAs. In the following, we briefly review recent advances in the design and demonstration of a more complex class of UWB discrete Raman amplifiers (DRAs) based on a dual-stage design approach [95] and also recent achievements in the application of machine learning techniques to the design of MB Raman amplifiers [96]. To increase the system OSNR, the so-called distributed Raman amplification is widely used, which, in its simplest form, comprises a number of high-power pumps multiplexed together and then coupled into the transmission fiber in a counterpropagating, or backward-pumped, configuration. However, to provide UWB gain, it is desirable to use a discrete, or lumped, Raman amplifier configuration, where all amplifier elements are located at the amplifier node [97]. Such a DRA does not provide the NF benefits of distributed amplification, but it is functionally equivalent to a conventional EDFA. Moreover, it enables the use of a specialty nonlinear fiber as the Raman gain medium, leading to increased pump efficiency, and has the added safety benefit of not requiring a pump light in the operator's fiber plant.

C. Mitigation of Transceiver Impairments

When it comes to the design of transceivers for UWB systems, there are, in principle, two design approaches: 1) design transceiver components specifically for UWB operation, i.e., covering several optical bands by a single device and 2) design individual components optimized for operation over a single optical band. While option 1) will certainly simplify stock-keeping since a single transceiver type can cover all bands, option 2) will enable better performance as transceivers only cover a single band, thus simplifying the optimized transceiver design. As outlined in Section III, transmitter and receiver components specifically developed for UWB operation, i.e., covering several optical bands by a single device, are still lacking. In particular, the following main components for optical UWB transceivers are not available as commercial products:

1) UWB tunable laser;
2) UWB dual-polarization IQ modulator;
3) UWB coherent receiver front end.

First, the characterization of a UWB silicon photonics integrated transmitter and receiver showed that operation over 370 nm of bandwidth using a single device is, in principle, possible [98], [99]. However, since then, there was little to no progress reported (cf. overviews in [100] and [101]). While specifically developed UWB transceiver components are widely unavailable, experimental investigation, in particular of $S + C + L$-band transmissions, currently relies mainly on C-band components, which are used out-of-band, coupled with digital mitigation schemes to cope with increased component-induced distortions. Section IV-C provides an overview of recent works on transmitter components and the related DSP. Another option to cope with the unavailability of UWB components, which is based on optical signal processing and wavelength conversion, is presented in Section IV-D.

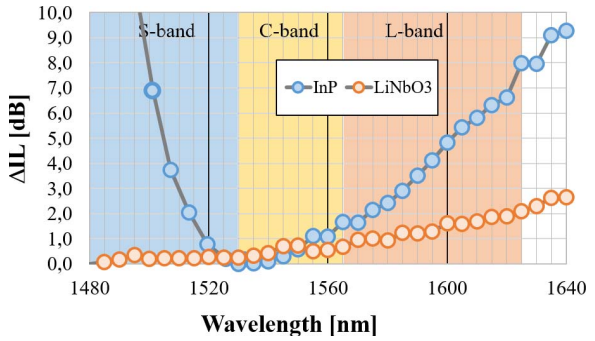

Fig. 9. ***Measured variation of IL (ΔIL) of exemplary commercially available InP and $LiNbO_3$ C-band modulators in S-, C-, and L-bands. In order to include wavelength dependency of modulation-induced loss, the measurements were performed under modulation conditions with 64-GBd dual-polarization 64-QAM signals.***

In principle, silicon photonics modulators can provide UWB modulation due to the broadband nature of the plasma dispersion effect [98], [99], [101]. However, the only published results date back to 2016, and comprehensive performance analysis is still lacking. In addition to silicon, lithium niobate ($LiNbO_3$) and indium phosphide (InP) modulators are potential candidates for UWB modulation. Recently, a simulative study has evaluated several InP modulator designs [102]. One of the critical building blocks for UWB operation of InP is the integrated beam splitters usually implemented in the form of multimode interference (MMI) couplers. Due to the wavelength dependence of the MMI splitting ratio, their operation over a wide wavelength range can lead to significant variations in terms of insertion loss (IL), power imbalance, and phase error of the modulator [103]. These variations can lead to unacceptable penalties [102]. However, initial results show that proper InP MMI designs can achieve a low variation of the splitting ratio and, thus, a high spectrum availability with low penalty [102]. An overview on the current state of the art of UWB modulator devices is presented in a companion paper devoted to UWB devices in this special issue [78]. Here, we focus on the system aspects of UWB modulator operation. Due to the unavailability of UWB modulators, there have been efforts to use C-band modulators in UWB operation over the S-, C-, and L-bands and quantify their performance [104]. Depending on the material and design of the C-band modulators, there may be large differences in their suitability for out-of-band use. As an example, Fig. 9 shows the measured variation of IL of two exemplary commercially available dual-polarization I/Q modulators: one based on $LiNbO_3$ and the other on InP. The measurements consider the IL under modulation conditions (dual-polarization 64-QAM, symbol rate of 64 GBd, and root-raised cosine pulse shape with 0.1 roll-off factor). In contrast to a CW measurement of the intrinsic IL, the modulation signal uses the full electrooptic bandwidth of the modulator. This way, the depicted variation of IL also includes the variation of the modulation-induced loss with wavelength. While the IL of the $LiNbO_3$ modulator is quite stable across the $S + C + L$-band, showing a variation of <2 dB, the InP modulator exhibits more than 10-dB variation. This has an important impact on the system performance since the IL influences the maximum transmitter output power and, thus, the achievable GSNR [see (1)].

In addition to the individual components, the DSP, which is performed at the transmitter and receiver sides, also needs to be adapted to UWB operation. For components operating over a wide wavelength range covering multiple bands, component specifications are expected to show a larger spread than only single-band conventional C-band operation. Advanced impairment estimation and compensation algorithms may help relax component specifications sufficiently to enable O- to L-band operations. In the past, there have already been various works, focusing on the compensation of transmitter impairments in the C-band by applying digital predistortion techniques. Such techniques play an important part in system design as they improve the AIR of a system by removing limitations due to transmitter components [105]. Recently, an approach for autonomous nonlinear system identification and transmitter predistortion based on hyperparameter tuning by the Bayesian optimization was proposed [106], [107]. The proposed scheme enables on-the-fly per-wavelength nonlinear system identification and predistortion of the whole transmitter subsystem, including digital-to-analog converters, driver amplifiers, and modulators. The autonomous digital predistortion scheme was evaluated in an $S + C + L$-band transmission scenario [108]. Although a significant performance gain was achieved, the performance in the lower S-band is still degraded compared with the C-band, as shown in Fig. 10, which displays the measured Q-factor in the $S + C + L$-band for linear and nonlinear predistortions

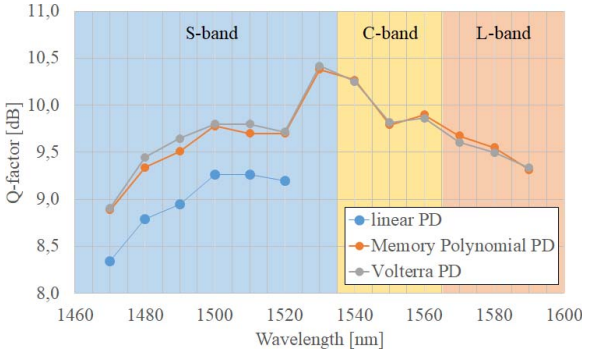

Fig. 10. ***Compensation of transmitter impairments by different digital predistortion techniques and per-wavelength autonomous optimization of filter design and coefficients (64-GBd DP-32-QAM, $LiNbO_3$ DP-IQM).***

either using a Volterra [109] or a reduced-complexity memory polynomial [110] nonlinear predistortion filter.

D. Whole Band Wavelength Conversion

As mentioned earlier in this article, it is not necessarily straightforward to develop optical components that support the full UWB spectrum. In particular, tunable lasers and optical amplifiers could be the most challenging components that should face certain limits of gain bandwidth defined by the material properties. Consequently, it becomes reasonable that the building blocks of a UWB network would start to use a mix of different types of devices, each of them covering a certain portion of the UWB spectrum (such as the one in Fig. 8, for instance). Such architecture should also be beneficial from the viewpoint of initial investment to the line-system optics because the network can be constructed in a limited number of bands with a small initial investment, and incremental capacity enhancement can be achieved by introducing additional optical components for additional bands.

However, this architecture still suffers from two issues: higher operational complexity and higher equipment cost. The operation complexity originates in the mixed use of different components that correspond to different bands. Extra attention should be necessary during the network construction, upgrade, or reconstruction for similar-looking devices for different bands that have to be connected to appropriate ports. Network operators should maintain a sufficient amount of inventory for possible upgrades or replacements for each component to cover different bands. Regarding the higher equipment cost, the new-band or UWB component should be limited in their production quantity, and thus. the cost reduction should be more challenging compared with C-band components where the production volume should be larger. This cost issue should be critical, particularly with transceivers that are by far the largest in quantity among various network elements.

All-optical wavelength conversion technology that translates optical signals from one wavelength band to another can be considered as a solution to the aforementioned issues. As schematically shown in Fig. 11, a virtual subsystem for a new band (i.e., the X-band) can be realized by inserting the whole band wavelength converter(s) at the optical input and/or output port(s) of an existing C-band subsystem. This idea should be most effective when it is applied to the WDM transceivers because one converter can translate the whole WDM spectrum in the C-band to the X-band or vice versa altogether.

Among numerous wavelength conversion techniques reported in the past [111], the whole band wavelength converter to be used here is required to be inherently transparent to the signal: being agnostic to the number of channels in the WDM signal, symbol rate, and modulation format of each channel and signal polarization, including the compatibility of polarization multiplexing. As a

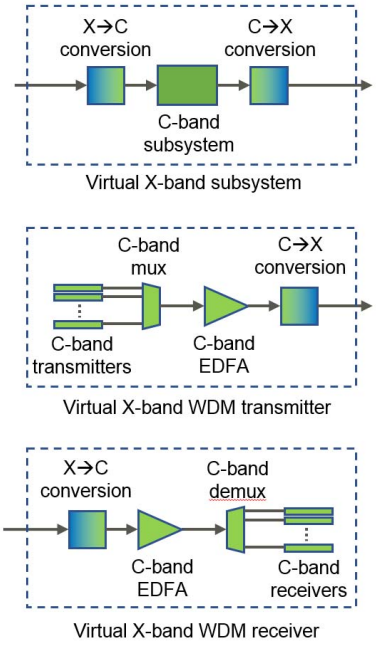

Fig. 11. ***Concept of new band subsystems based on C-band components and whole band wavelength conversion. Top: virtual X-band in-line subsystem. Middle: virtual X-band WDM transmitter. Bottom: virtual X-band WDM receiver.***

candidate to satisfy such requirements, highly nonlinear fiber has been considered as one of the most promising media to generate wavelength-translated idler through FWM between the input WDM signal and continuous-wave pump light(s) at one or two wavelength(s) [112]. Collective wavelength conversion without modulation format and polarization sensitivity was demonstrated with a highly nonlinear fiber incorporated in the polarization diversity configuration [113]. Note that the fiber nonlinearity, which is usually a source of signal impairment in a fiber-optic transmission system, plays a key role to provide new network functionality. Two main basic parameters that characterize the performance of the whole band wavelength converter are conversion efficiency and conversion bandwidth.

More recently, this technique was utilized to propose and demonstrate a UWB transmission system by adopting the concept depicted in Fig. 11 [74], [114]. The proposed system comprises, in addition to multiple sets of C-band WDM transceivers and a transmission line, a wavelength-band multiplexer/demultiplexer and a pair of wavelength converters that enable the virtual use of C-band WDM transceivers as X-band transceiver. With this scheme, UWB WDM transmission systems can be developed without transceivers operating in new bands but C-band transceivers that are more mature and at the forefront of new development (see Fig. 12). An experimental demonstration of this system concept was given in a triple-band ($S + C + L$-band) with 200-Gb/s (34-GBd DP-16-QAM) test signals in 50-GHz spacing. The C-band WDM signal was translated by a wavelength converter having the

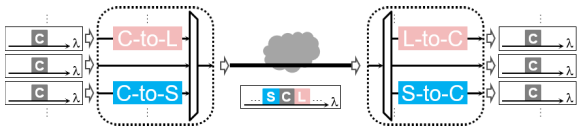

Fig. 12. *Schematic of the UWB transmission system using whole band wavelength conversion. Tx: transceiver.*

characteristics shown in Fig. 13(a) and (b). They were then multiplexed with the other WDM signal in the C-band to generate a triple-band WDM signal. The signal quality after the 40-km standard SMF transmission was received by a real-time digital coherent receiver in the C-band after band demultiplexing and wavelength conversion back into the C-band in the same configuration as that of the transmitter side [see Fig. 13(c) and (d)], where no bit error was observed after performing forward error correction on all 240 channels.

Whole band wavelength conversion can play other roles in future optical networks by providing advanced functionality. Such functionality can include amplification [115], MB protection and bidirectional transmission [116], and transmission performance improvement by equalizing the signal quality by wavelength-band switching within a multispan transmission system [117].

Major characteristics that determine the performance of the whole band wavelength converter are conversion bandwidth and conversion efficiency. Regarding the conversion bandwidth, the key limiting factor is the phase matching among the input signal, pump light, and wavelength-converted idler across a wide wavelength range. The conversion bandwidth can be extended by using a shorter length of a nonlinear fiber [118], but group velocity tailoring of the nonlinear fiber [119] should be necessary to develop it with a practical pump light power of less than 1 W. Regarding conversion efficiency, it is important to have a conversion with minimal loss across the wavelength band to avoid OSNR degradation in the network. Although the conversion efficiency is determined by the product of the nonlinear coefficient, the pump power, and the effective length of the nonlinear medium, its upper limit is capped by the saturation characteristics of the nonlinear medium. In wavelength conversion based on highly nonlinear fiber, stimulated Brillouin scattering (SBS) sets a limit to the pump power. The limitation imposed by SBS can be mitigated by broadening the spectral width of the pump light launched into the nonlinear fiber, and thus, the conversion efficiency can be improved [120]. A potential problem in the coherent reception of the wavelength converted signal with the spectrally broadened pump light can be mitigated by a dual-pump configuration with synchronous frequency dithering [121], [122] and can be considered to minimize such a penalty.

Further applications of wavelength conversion can be enabled by different types of nonlinear media in addition to the highly nonlinear fiber. One possible candidate should be a highly efficient nonlinear medium that can provide a conversion gain such as periodically poled $LiNbO_3$ waveguide [89]. The nonlinear waveguide using silicon-based semiconductor waveguide [123], [124], [125] is another interesting platform with a potential toward low power consumption and highly functional integration in the future.

E. Transmission in Hollow Core Fiber

As an alternative to SMF, and to solid-core fibers, in general, HCFs were proposed in the 1990s [126]. However, for many years, HCFs' loss remained very high, and their usable optical bandwidth appeared to be relatively limited. The situation changed with the advent of HCFs of the NANF type, proposed in 2014 [25]. While the first fabricated NANFs still had a high loss, steadily decreasing loss values were obtained in the following years. In 2019, the 1-dB/km mark was reached, and recently, a breakthrough value of 0.174 dB/km over the C-band [26] has been reported. The results in [26] also indicate that, if the water peak was eliminated, the loss could be less than 0.23 dB/km over 300+ nm and less than 0.3 dB/km over 400+ nm. Further improvement appears possible, too.

In addition to the low loss and large bandwidth, NANF also enjoys a Kerr nonlinearity coefficient γ, which is three to four orders of magnitude lower than SMF, due to the propagation in NANF occurring in gas. This means that both NLI and SRS are practically negligible in NANF, which behaves essentially as a linear medium. Another positive aspect of NANF is that its chromatic dispersion is low, about 2.5 ps/(nm · km). This could substantially ease the DSP effort for dispersion compensation, especially at the ultrahigh symbol rates that are currently being developed. Another advantage of NANF is that light propagates at almost vacuum speed. The reduction of propagation time is attractive for certain applications where latency is important.

One critical aspect of NANF is intermodal interference (IMI), which may occur because NANFs are intrinsically multimodal and achieve single-mode operation thanks to higher order modes having large attenuation. If this mechanism of mode suppression is not effective, then substantial IMI can be present, which may cause a significant

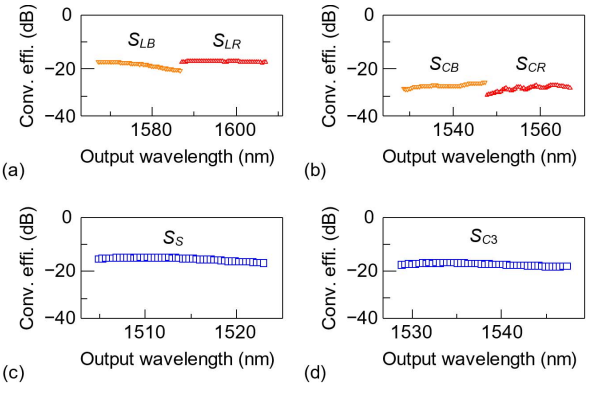

Fig. 13. *Measured conversion efficiency of wavelength conversion for (a) C-to-L, (b) L-to-C, (c) C-to-S, and (d) S-to-C.*

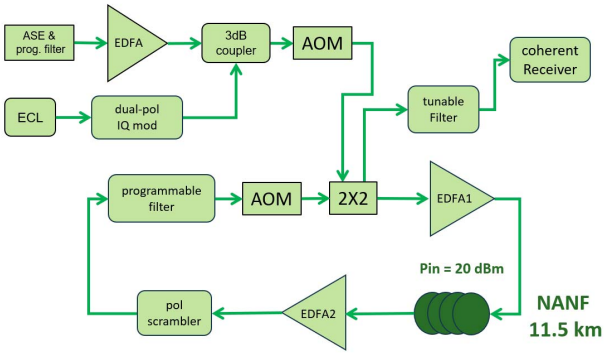

Fig. 14. ***Schematic of the NANF recirculating loop experiment [128].***

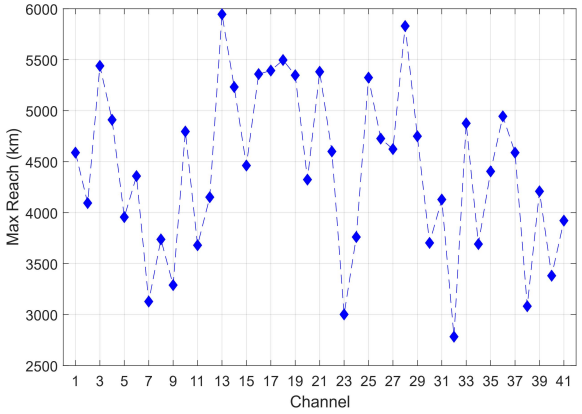

Fig. 15. ***Maximum reach of each individual channel of the experiment [128] whose schematic is shown in Fig. 14. The transmission was PM-QPSK at 32 GBd.***

transmission penalty. The threshold for the negligible impact of IMI is estimated to be about −60 dB/km [127].

To test the behavior of NANFs in actual long-haul transmission, various recirculating loop experiments have been carried out. The longest reach [128] involved transmission of 41 PM-QPSK channels over 4000 km of NANF at an average per-channel generalized mutual information (GMI) of 3.54 bit/symbol. A variant of the same experiment [128] characterized each individual channel's maximum reach (with all others still being transmitted). Maximum reach was defined as the maximum distance for which the channel GMI was ≥3.5 bit/symbol. Fig. 14 shows the schematic of the experiment. Notice that the available NANF length was only 11.5 km. The results are shown in Fig. 15. Remarkably, some channels approached 6000 km, which corresponds to over 500 turns in the recirculating loop. Several exceeded 5000 km. On the other hand, a few channels reached only about 3000 km. This discrepancy in results was partly explained by disuniformity in the spectral response of the loop at the hundreds of recirculations that were being used, beyond the capability of the loop programmable filter resolution to cope with. Partly, it was attributed to nonnegligible IMI, which was estimated to be about −50 dB/km. This value was confirmed by independent direct measurement of the NANF, carried out by means of a sliding window and Fourier filtering analysis of the transmission spectrum [129].

The experiment [128] showed very significant progress versus previous experiments, proving that NANF was on a quick development trend. This trend was confirmed by the latest NANF specimen, presented in the already mentioned recent paper [26], which far outperforms the NANF used in [128]: a loss of 0.174 dB/km in [26] versus 0.8 dB/km in the experiment [128]. In addition, the IMI of the NANF [26] has been measured to be between −54 and −58 dB/km, hence close to the −60 dB/km required for virtually no IMI impact. It can, therefore, be expected that, when the latest generation NANF is used in a long-haul experiment, better results and better uniformity among channels than [128] could be found. It should also be noted that an important condition for NANF to deliver new record long-haul performance is that long stretches of fiber can be fabricated. Performing recirculating loop experiments over only a few km of fiber clearly makes experimentation difficult and introduces substantial setup-related spurious effects.

The potential of future NANFs to deliver a possibly larger throughput than SMF was theoretically investigated in [127]. It was found that, over 1000-km links (10 × 100 km), NANF could deliver up to 5×–6× the throughput of a Raman-amplified (with 0-dB NF) SMF $C + L$ system, assuming an NANF loss of 0.2 dB/km across 400 nm of bandwidth and lumped amplification with an NF of 9 dB. Note that realizing such systems would require exceptional progress in many aspects: cost-effective top-performance NANF fabrication in quantity; suitable optical amplification and optical sources across hundreds of nm; and development of many ancillary technologies needed for practical deployment. These are very substantial challenges. Nonetheless, the peculiar features of NANF are quite attractive and might make it a possible future contender for UWB systems.

V. CONCLUSION

The fiber capacity growth that has been achieved over the last three decades has resulted primarily from increasing the SE while using the same amplifier bandwidth. However, we are approaching the nonlinear Shannon limit, and this approach to scaling capacity is being rapidly exhausted. Future system scaling will come through provisioning more bandwidth either in the form of a wider spectrum on a single fiber as discussed here or through copies of the existing spectrum on multiple spatial channels, as described in other papers in this issue. Given the diversity of locations and constraints on optical fiber systems, both approaches will likely be applicable in future networks. Extension of the optical bandwidth beyond the $C + L$-band is, therefore, expected to play a significant role in upgrading the capacity of future optical networks.

In this article, we have considered the merits and challenges of a UWB optical transport system beyond

conventional bands to meet this expected capacity growth. We have identified technologies and application areas where UWB may have a significant impact. We reviewed the state-of-the-art UWB system demonstrations, their enabling technologies, and unique technical issues to UWB systems, such as system modeling and design, transceiver impairments, and optical amplification technologies. We also looked at a new type of fiber, hollow-core NANF, which might provide future ultrawide bandwidths with negligible non-linearity. Furthermore, using whole band wavelength conversion was reviewed as a potential means to overcome cost-related challenges in the UWB network. This has the potential to allow the reuse of current conventional band components, which would overcome the time and costs required to develop transmit and receive components for all the new bands. ■

REFERENCES

[1] P. J. Winzer, D. T. Neilson, and A. R. Chraplyvy, "Fiber-optic transmission and networking: The previous 20 and the next 20 years [Invited]," *Opt. Exp.*, vol. 26, no. 18, pp. 24190–24239, Sep. 2018, doi: 10.1364/OE.26.024190.

[2] R. J. Mears, L. Reekie, I. M. Jauncey, and D. N. Payne, "Low-noise erbium-doped fibre amplifier operating at 1.54 μm," *Electron. Lett.*, vol. 23, no. 19, pp. 1026–1028, Sep. 1987, doi: 10.1049/el:19870719.

[3] E. Desurvire, J. R. Simpson, and P. C. Becker, "High-gain erbium-doped traveling-wave fiber amplifier," *Opt. Lett.*, vol. 12, no. 11, pp. 888–890, Nov. 1987, doi: 10.1364/OL.12.000888.

[4] M. Nakazawa, Y. Kimura, and K. Suzuki, "Efficient Er^{3+}-doped optical fiber amplifier pumped by a 1.48 μm InGaAsP laser diode," *Appl. Phys. Lett.*, vol. 54, no. 4, pp. 295–297, 1989, doi: 10.1063/1.101448.

[5] *Transmission Systems and Media, Digital Systems and Networks*, document ITU-T G.Sup39, Feb. 2016.

[6] M. Jinno *et al.*, "First demonstration of 1580 nm wavelength band WDM transmission for doubling usable bandwidth and suppressing FWM in DSF," *Electron. Lett.*, vol. 33, no. 10, pp. 882–883, May 1997, doi: 10.1049/el:19970584.

[7] Y. Sun *et al.*, "An 80 nm ultra wide band EDFA with low noise figure and high output power," in *Proc. Integr. Optics Opt. Fibre Commun., 11th Int. Conf., 23rd Eur. Conf. Opt. Commun.*, vol. 5, Sep. 1997, pp. 69–72.

[8] J. F. Massicott, J. R. Armitage, R. Wyatt, B. J. Ainslie, and S. P. Craig-Ryan, "High gain, broadband, 1.6 μm Er^{3+} doped silica fibre amplifier," *Electron. Lett.*, vol. 26, no. 20, pp. 1645–1646, 9 1990.

[9] H. Ono, M. Yamada, and Y. Ohishi, "Gain-flattened Er^{3+}-doped fiber amplifier for a WDM signal in the 1.57-1.60-μm wavelength region," *IEEE Photon. Technol. Lett.*, vol. 9, no. 5, pp. 596–598, May 1997.

[10] J. Kani, K. Hattori, M. Jinno, T. Kanamori, and K. Oguchi, "Triple-wavelength-band WDM transmission over cascaded dispersion-shifted fibers," *IEEE Photon. Technol. Lett.*, vol. 11, no. 11, pp. 1506–1508, Nov. 1999.

[11] E. Ishikawa, M. Nishihara, Y. Sato, C. Ohshima, Y. Sugaya, and J. Kumasako, "Novel 1500 nm-band EDFA with discrete Raman amplifier," in *Proc. 27th Eur. Conf. Opt. Commun.*, Sep./Oct. 2001.

[12] K. Fukuchi *et al.*, "10.92-Tb/s (273×40-Gb/s) triple-band/ultra-dense WDM optical-repeatered transmission experiment," in *Proc. Opt. Fiber Commun. Conf.*, 2001, p. PD24.

[13] T. Tanaka, K. Torii, M. Yuki, H. Nakamoto, T. Naito, and I. Yokota, "200-nm bandwidth WDM transmission around 1.55 μm using distributed Raman amplifier," in *Proc. 28th Eur. Conf. Opt. Commun.*, vol. 5, 2002, p. PD4.6.

[14] C. E. Shannon, "A mathematical theory of communication," *Bell Syst. Tech. J.*, vol. 27, no. 3, pp. 379–423, Jul. 1948.

[15] X. Liu, "Evolution of fiber-optic transmission and networking toward the 5G era," *iScience*, vol. 22, pp. 489–506, Dec. 2019.

[16] D. A. Fishman, W. A. Thompson, and L. Vallone, "LambdaXtreme transport system: R&D of a high capacity system for low cost, ultra long haul DWDM transport," *Bell Labs Tech. J.*, vol. 11, no. 2, pp. 27–53, Summer 2006.

[17] V. Vusirikala, X. Zhao, T. Hofmeister, V. Kamalov, V. Dangui, and B. Koley, "Scalable and flexible transport networks for inter-datacenter connectivity," in *Proc. Opt. Fiber Commun. Conf.*, 2015, pp. 1–3, Paper Tu3H.1.

[18] M. Cantono, R. Schmogrow, M. Newland, V. Vusirikala, and T. Hofmeister, "Opportunities and challenges of C+L transmission systems," *J. Lightw. Technol.*, vol. 38, no. 5, pp. 1050–1060, Mar. 1, 2020.

[19] A. Ferrari *et al.*, "Assessment on the achievable throughput of multi-band ITU-T G.652.D fiber transmission systems," *J. Lightw. Technol.*, vol. 38, no. 16, pp. 4279–4291, Aug. 15, 2020, doi: 10.1109/JLT.2020.2989620.

[20] G. Agrawal, *Nonlinear Fiber Optics*. Amsterdam, The Netherlands: Elsevier, 2007, doi: 10.1007/3-540-46629-0_9.

[21] D. Marcuse, A. R. Chraplyvy, and R. W. Tkach, "Dependence of cross-phase modulation on channel number in fiber WDM systems," *J. Lightw. Technol.*, vol. 12, no. 5, pp. 885–890, May 1994, doi: 10.1109/50.293982.

[22] R. Essiambre, G. Kramer, P. J. Winzer, G. J. Foschini, and B. Goebel, "Capacity limits of optical fiber networks," *J. Lightw. Technol.*, vol. 28, no. 4, pp. 662–701, Feb. 15, 2010, doi: 10.1109/JLT.2009.2039464.

[23] R. H. Stolen, E. P. Ippen, and A. R. Tynes, "Raman oscillation in glass optical waveguide," *Appl. Phys. Lett.*, vol. 20, no. 2, pp. 62–64, 1972, doi: 10.1063/1.1654046.

[24] H. Kidorf, K. Rottwitt, M. Nissov, M. Ma, and E. Rabarijaona, "Pump interactions in a 100-nm bandwidth Raman amplifier," *IEEE Photon. Technol. Lett.*, vol. 11, no. 5, pp. 530–532, May 1999, doi: 10.1109/68.759388.

[25] F. Poletti, "Nested antiresonant nodeless hollow core fiber," *Opt. Exp.*, vol. 22, no. 20, pp. 23807–23828, 2014, doi: 10.1364/OE.22.023807.

[26] G. T. Jasion *et al.*, "0.174 dB/km hollow core double nested antiresonant nodeless fiber (DNANF)," in *Proc. Opt. Fiber Commun. Conf. (OFC)*, 2022, pp. 1–3, Paper Th4.C.7.

[27] A. Mecozzi and R.-J. Essiambre, "Nonlinear Shannon limit in pseudolinear coherent systems," *J. Lightw. Technol.*, vol. 30, no. 12, pp. 2011–2024, Jun. 15, 2012, doi: 10.1109/JLT.2012.2190582.

[28] R. Dar, M. Feder, A. Mecozzi, and M. Shtaif, "Properties of nonlinear noise in long, dispersion-uncompensated fiber links," *Opt. Exp.*, vol. 21, no. 22, pp. 25685–25699, 2013, doi: 10.1364/OE.21.025685.

[29] P. Poggiolini, G. Bosco, A. Carena, V. Curri, Y. Jiang, and F. Forghieri, "The GN-model of fiber non-linear propagation and its applications," *J. Lightw. Technol.*, vol. 32, no. 4, pp. 694–721, Feb. 15, 2014, doi: 10.1109/JLT.2013.2295208.

[30] A. Carena, G. Bosco, V. Curri, Y. Jiang, P. Poggiolini, and F. Forghieri, "EGN model of non-linear fiber propagation," *Opt. Exp.*, vol. 22, no. 13, pp. 16335–16362, 2014, doi: 10.1364/OE.22.016335.

[31] R. Dar, M. Feder, A. Mecozzi, and M. Shtaif, "Accumulation of nonlinear interference noise in fiber-optic systems," *Opt. Exp.*, vol. 22, no. 12, pp. 14199–14211, Jun. 2014, doi: 10.1364/OE.22.014199.

[32] V. Curri, "Software-defined WDM optical transport in disaggregated open optical networks," in *Proc. 22nd Int. Conf. Transparent Opt. Netw. (ICTON)*, Jul. 2020, pp. 1–4, doi: 10.1109/ICTON51198.2020.9203450.

[33] A. Bononi, O. Beucher, and P. Serena, "Single- and cross-channel nonlinear interference in the Gaussian noise model with rectangular spectra," *Opt. Exp.*, vol. 21, no. 26, pp. 32254–32268, Dec. 2013, doi: 10.1364/OE.21.032254.

[34] M. Filer, M. Cantono, A. Ferrari, G. Grammel, G. Galimberti, and V. Curri, "Multi-vendor experimental validation of an open source QoT estimator for optical networks," *J. Lightw. Technol.*, vol. 36, no. 15, pp. 3073–3082, Aug. 1, 2018, doi: 10.1109/JLT.2018.2818406.

[35] A. Pilipetskii *et al.*, "The subsea fiber as a Shannon channel," in *Proc. SubOptic*, 2019, pp. 1–7, Paper OP12-2. [Online]. Available: https://suboptic2019.com/download/5176/

[36] A. Ferrari *et al.*, "GNPy: An open source application for physical layer aware open optical networks," *J. Opt. Commun. Netw.*, vol. 12, no. 6, p. C31, 2020, doi: 10.1364/JOCN.382906.

[37] V. Curri *et al.*, "Design strategies and merit of system parameters for uniform uncompensated links supporting Nyquist-WDM transmission," *IEEE/OSA J. Lightw. Technol.*, vol. 33, no. 18, pp. 3921–3932, Jun. 2015, doi: 10.1109/JLT.2015.2447151.

[38] A. D'Amico *et al.*, "GNPy experimental validation on flex-grid, flex-rate WDM optical transport scenarios," in *Proc. Opt. Fiber Commun. Conf. (OFC)*, 2021, pp. 1–3, Paper W1G.2

[39] H. Sun *et al.*, "800G DSP ASIC design using probabilistic shaping and digital sub-carrier multiplexing," *J. Lightw. Technol.*, vol. 38, no. 17, pp. 4744–4756, Sep. 1, 2020, doi: 10.1364/JLT.38.004744.

[40] F. P. Guiomar, R. Li, C. R. S. Fludger, A. Carena, and V. Curri, "Hybrid modulation formats enabling elastic fixed-grid optical networks," *J. Opt. Commun. Netw.*, vol. 8, no. 7, p. A92, 2016, doi: 10.1364/JOCN.8.000A92.

[41] J. Cho and P. J. Winzer, "Probabilistic constellation shaping for optical fiber communications," *J. Lightw. Technol.*, vol. 37, no. 6, pp. 1590–1607, Mar. 15, 2019, doi: 10.1109/JLT.2019.2898855.

[42] V. Curri and A. Carena, "Merit of Raman pumping in uniform and uncompensated links supporting NyWDM transmission," *J. Lightw. Technol.*, vol. 34, no. 2, pp. 554–565, Jan. 2015, doi: 10.1109/JLT.2015.2477599.

[43] E. Ip and J. M. Kahn, "Compensation of dispersion and nonlinear impairments using digital backpropagation," *J. Lightw. Technol.*, vol. 26, no. 20, pp. 3416–3425, Oct. 15, 2008, doi: 10.1109/JLT.2008.927791.

[44] D. Marcuse, C. R. Manyuk, and P. K. A. Wai, "Application of the Manakov-PMD equation to studies of signal propagation in optical fibers with randomly varying birefringence," *J. Lightw. Technol.*, vol. 15, no. 9, pp. 1735–1746, Sep. 1997, doi: 10.1109/50.622902.

[45] J. E. Aber, M. C. Newstein, and B. A. Garetz, "Femtosecond optical Kerr effect measurements in silicate glasses," *J. Opt. Soc. Amer. B, Opt. Phys.*, vol. 17, no. 1, pp. 120–127, 2000, doi: 10.1364/JOSAB.17.000120.

[46] S. Walker, "Rapid modeling and estimation of total spectral loss in optical fibers," *J. Lightw. Technol.*, vol. 4, no. 8, pp. 1125–1131, Aug. 1986, doi: 10.1109/JLT.1986.1074874.

[47] G. Borraccini *et al.*, "Cognitive and autonomous QoT-driven optical line controller," *J. Opt. Commun. Netw.*, vol. 13, no. 10, pp. E23–E31, 2021, doi: 10.1364/JOCN.424021.

[48] C. R. S. Fludger, V. Handerek, and R. J. Mears, "Pump to signal RIN transfer in Raman fiber amplifiers," *J. Lightw. Technol.*, vol. 19, no. 8, pp. 1140–1148, Aug. 2001, doi: 10.1109/50.939794.

[49] K. Rottwitt, J. Bromage, A. J. Stentz, L. Leng, M. E. Lines, and H. Smith, "Scaling of the Raman gain coefficient: Applications to germanosilicate fibers," *J. Lightw. Technol.*, vol. 21, no. 7, p. 1652, Jul. 1, 2003, doi: 10.1109/JLT.2003.814386.

[50] N. Sambo *et al.*, "Multiband seamless network upgrade by exploiting the E-band," in *Proc. Eur. Conf. Opt. Commun. (ECOC)*, Sep. 2021, pp. 1–4.

[51] F. Vanholsbeeck, S. Coen, P. Emplit, M. Haelterman, and T. Sylvestre, "Raman-induced power tilt in arbitrarily large wavelength-division-multiplexed systems," *IEEE Photon. Technol. Lett.*, vol. 17, no. 1, pp. 88–90, Jan. 2005.

[52] J. Bromage, "Raman amplification for fiber communications systems," *J. Lightw. Technol.*, vol. 22, no. 1, p. 79, Jan. 1, 2004, doi: 10.1109/JLT.2003.822828.

[53] M. Cantono *et al.*, "On the interplay of nonlinear interference generation with stimulated Raman scattering for QoT estimation," *J. Lightw. Technol.*, vol. 36, no. 15, pp. 3131–3141, Aug. 1, 2018, doi: 10.1109/JLT.2018.2814840.

[54] D. Semrau, R. I. Killey, and P. Bayvel, "The Gaussian noise model in the presence of inter-channel stimulated Raman scattering," *J. Lightw. Technol.*, vol. 36, no. 14, pp. 3046–3055, Jul. 15, 2018, doi: 10.1109/JLT.2018.2830973.

[55] B. Correia *et al.*, "Power control strategies and network performance assessment for C+L+S multiband optical transport," *J. Opt. Commun. Netw.*, vol. 13, no. 7, pp. 147–157, Jul. 2021, doi: 10.1364/JOCN.419293.

[56] V. Oliari, E. Agrell, and A. Alvarado, "Regular perturbation on the group-velocity dispersion parameter for nonlinear fibre-optical communications," *Nature Commun.*, vol. 11, no. 1, Dec. 2020, doi: 10.1038/s41467-020-14503-w.

[57] M. Eiselt, R. M. Jopson, and R. H. Stolen, "Nondestructive position-resolved measurement of the zero-dispersion wavelength in an optical fiber," *J. Lightw. Technol.*, vol. 15, no. 1, pp. 135–143, Jan. 1997, doi: 10.1109/50.552121.

[58] B. J. Puttnam, R. S. Luís, G. Rademacher, M. Mendez-Astudilio, Y. Awaji, and H. Furukawa, "S, C and extended L-band transmission with doped fiber and distributed Raman amplification," in *Proc. Opt. Fiber Commun. Conf. Exhib.*, 2021, pp. 1–3, Paper Th4C.2.

[59] L. Galdino *et al.*, "Optical fibre capacity optimisation via continuous bandwidth amplification and geometric shaping," *IEEE Photon. Technol. Lett.*, vol. 32, no. 17, pp. 1021–1024, Sep. 1, 2020, doi: 10.1109/LPT.2020.3007591.

[60] F. Hamaoka *et al.*, "150.3-Tb/s ultra-wideband (S, C, and L bands) single-mode fibre transmission over 40-km using >519Gb/s/A PDM-128QAM signals," in *Proc. Eur. Conf. Opt. Commun.*, 2018, pp. 1–3, Paper Mo4G.1, doi: 10.1109/ECOC.2018.8535140.

[61] J. Renaudier *et al.*, "First 100-nm continuous-band WDM transmission system with 115Tb/s transport over 100 km using novel ultra-wideband semiconductor optical amplifiers," in *Proc. 43rd Eur. Conf. Opt. Commun.*, 2017, pp. 1–3, Paper Th.PDP.A.3, doi: 10.1109/ECOC.2017.8346084.

[62] A. Sano *et al.*, "102.3-Tb/s (224×548-Gb/s) C- and extended L-band all-Raman transmission over 240 km using PDM-64QAM single carrier FDM with digital pilot tone," in *Proc. Nat. Fiber Opt. Eng. Conf.*, 2012, pp. 1–3, Paper PDP5C.3, doi: 10.1364/NFOEC.2012.PDP5C.3.

[63] J. Renaudier *et al.*, "107 Tb/s transmission of 103-nm bandwidth over 3×100 km SSMF using ultra-wideband hybrid Raman/SOA repeaters," in *Proc. Opt. Fiber Commun. Conf.*, 2019, pp. 1–3, Paper Tu3F.2, doi: 10.1364/OFC.2019.Tu3F.2.

[64] L. Galdino *et al.*, "Study on the impact of nonlinearity and noise on the performance of high-capacity broadband hybrid Raman-EDFA amplified system," *J. Lightw. Technol.*, vol. 37, no. 21, pp. 5507–5515, Nov. 1, 2019, doi: 10.1109/JLT.2019.2933246.

[65] J.-X. Cai *et al.*, "94.9 Tb/s single mode capacity demonstration over 1,900 km with C+L EDFAs and coded modulation," in *Proc. 44th Eur. Conf. Opt. Commun.*, 2018, pp. 1–3, Paper Mo4G.3, doi: 10.1109/ECOC.2018.8535554.

[66] M. Ionescu *et al.*, "74.38 Tb/s transmission over 6300 km single mode fibre enabled by C+L amplification and geometrically shaped PDM-64QAM," *J. Lightw. Technol.*, vol. 38, no. 2, pp. 531–537, Jan. 15, 2020, doi: 10.1109/JLT.2019.2954458.

[67] J.-X. Cai *et al.*, "70.46 Tb/s over 7,600 km and 71.65 Tb/s over 6,970 km transmission in C+L band using coded modulation with hybrid constellation shaping and nonlinearity compensation," *J. Lightw. Technol.*, vol. 36, no. 1, pp. 114–121, Jan. 1, 2018, doi: 10.1109/JLT.2017.2757281.

[68] J.-X. Cai *et al.*, "49.3 Tb/s transmission over 9100 km using C+L EDFA and 54 Tb/s transmission over 9150 km using hybrid-Raman EDFA," *J. Lightw. Technol.*, vol. 33, no. 13, pp. 2724–2734, Jul. 1, 2015.

[69] J.-X. Cai *et al.*, "51.5 Tb/s capacity over 17,107 km in C+L bandwidth using single-mode fibers and nonlinearity compensation," *J. Lightw. Technol.*, vol. 36, no. 11, pp. 2135–2141, Jan. 1, 2018, doi: 10.1109/JLT.2018.2802322.

[70] A. Napoli *et al.*, "Perspectives of multi-band optical communication systems," in *Proc. 23rd Opto-Electron. Commun. Conf. (OECC)*, Jul. 2018, pp. 1–2, Paper 5B3-1, doi: 10.1109/OECC.2018.8730026.

[71] B. Puttnam, R. Luis, G. Rademacher, Y. Awaji, and H. Furukawa, "319 Tb/s transmission over 3001 km with S, C and L band signals over >120 nm bandwidth in 125 μm wide 4-core fiber," in *Proc. Opt. Fiber Commun. Conf. Exhib.*, 2021, pp. 1–3, Paper F3B.3.

[72] J.-X. Cai *et al.*, "On the effects of transmitter induced channel correlation in broadband WDM transmission," in *Proc. Opt. Fiber Commun. Conf.*, 2018, pp. 1–3, Paper Th1C.1, doi: 10.1364/OFC.2018.Th1C.1.

[73] D. J. Elson *et al.*, "Investigation of bandwidth loading in optical fibre transmission using amplified spontaneous emission noise," *Opt. Exp.*, vol. 25, no. 16, pp. 19529–19537, Aug. 2017, doi: 10.1364/OE.25.019529.

[74] T. Kato *et al.*, "Real-time transmission of 240×200-Gb/s signal in S+C+L triple-band WDM without S- or L-band transceivers," in *Proc. 45th Eur. Conf. Opt. Commun.*, 2019, Paper PD1.7, doi: 10.1049/cp.2019.1021.

[75] H. Buglia, E. Sillekens, A. Vasylchenkova, P. Bayve, and L. Galdino, "On the impact of launch power optimization and transceiver noise on the performance of ultra-wideband transmission systems [Invited]," *J. Opt. Commun. Netw.*, vol. 14, no. 5, pp. B11–B21, May 2022, doi: 10.1364/JOCN.450726.

[76] J.-X. Cai, G. Mohs, and N. S. Bergano, "Ultralong-distance undersea transmission systems," in *Optical Fiber Telecommunications*, vol. 7, A. E. Willner, Ed. New York, NY, USA: Academic, 2020, ch. 13, pp. 565–625.

[77] P. Trischitta, M. Colas, M. Green, G. Wuzniak, and J. Arena, "The TAT-12/13 cable network," *IEEE Commun. Mag.*, vol. 34, no. 2, pp. 24–28, Feb. 1996.

[78] J. Renaudier *et al.*, "Devices and components for ultra-wideband optical communications," *Proc. IEEE*, to be published.

[79] B. C. Collings, "Advanced ROADM technologies and architectures," in *Proc. Opt. Fiber Commun. Conf.*, 2015, pp. 1–3, Paper Tu3D.3.

[80] H. Chen, N. K. Fontaine, B. Huang, X. Xiao, R. Ryf, and D. T. Neilson, "Wavelength selective switch for dynamic VCSEL-based data centers," in *Proc. 42nd Eur. Conf. Opt. Commun.*, 2016, pp. 1–3, Paper Th.3.B.1.

[81] N. K. Fontaine, M. Mazur, R. Ryf, H. Chen, L. Dallachiesa, and D. T. Neilson, "36-THz bandwidth wavelength selective switch," in *Proc. Eur. Conf. Opt. Commun. (ECOC)*, Sep. 2021, pp. 1–4, Paper Th3C1-PD2.3.

[82] Lightwave, Ed. (Mar. 2021). *Finisar WSS: Flexgrid(R) C+L Wavelength Selective Switch*. Accessed: Jul. 9, 2021. https://web.archive.org/web/20210709135938/ and https://www.lightwaveonline.com/test/design-manufacturing/article/14199805/finisar-wss-flexgridr-cl-wavelength-selective-switch

[83] L. Rapp and M. Eiselt, "Optical amplifiers for wideband optical transmission systems," in *Proc. Opt. Fiber Commun. Conf. (OFC)*, 2021, pp. 1–3, Paper Th4C.1.

[84] L. Rapp and M. Eiselt, "Ultra-wideband amplification strategies," in *Proc. IEEE Photon. Soc. Summer Topicals Meeting Ser. (SUM)*, Jul. 2021, pp. 1–2, doi: 10.1109/SUM48717.2021.9505858.

[85] A. Donodin *et al.*, "Bismuth doped fibre amplifier operating in E- and S- optical bands," *Opt. Mater. Exp.*, vol. 11, no. 1, pp. 127–135, 2021.

[86] V. Mikhailov *et al.*, "Simple broadband bismuth doped fiber amplifier (BDFA) to extend O-band transmission reach and capacity," in *Proc. Opt. Fiber Commun. Conf. Exhib.*, 2019, pp. 1–3, Paper M1J.4, doi: 10.1364/OFC.2019.M1J.4.

[87] J. Renaudier *et al.*, "Recent advances in 100+nm ultra-wideband fiber-optic transmission systems using semiconductor optical amplifiers," *J. Lightw. Technol.*, vol. 38, no. 5, pp. 1071–1079, Mar. 1, 2020, doi: 10.1109/JLT.2020.2966491.

[88] M. F. C. Stephens, M. Tan, V. Gordienko, P. Harper, and N. J. Doran, "In-line and cascaded DWDM transmission using a 15 dB net-gain polarization-insensitive fiber optical parametric amplifier," *Opt. Exp.*, vol. 25, no. 20, pp. 24312–24325, 2017, doi: 10.1364/OE.25.024312.

[89] T. Kobayashi *et al.*, "Wide-band inline-amplified WDM transmission using PPLN-based optical parametric amplifier," *J. Lightw. Technol.*, vol. 39, no. 3, pp. 787–794, Feb. 1, 2021, doi: 10.1109/JLT.2020.3039192.

[90] H. Masuda, M. Tomizawa, and Y. Miyamoto, "High-performance distributed Raman amplification systems: Practical aspects and field trial results," in *Proc. Opt. Fiber Commun. Conf.*, 2005, p. 3, Paper OThF5, doi: 10.1109/OFC.2005.192926.

[91] W. S. Pelouch, "Raman amplification: An enabling technology for long-haul coherent transmission systems," *J. Lightw. Technol.*, vol. 34, no. 1, pp. 6–19, Jan. 1, 2016, doi: 10.1109/JLT.2015.2458771.

[92] H. Bissessur, C. Bastide, S. Dubost, and S. Etienne, "80×200 Gb/s 16-QAM unrepeatered transmission over 321 km with third order Raman amplification," in *Proc. Opt. Fiber Commun. Conf.*, 2015, pp. 1–3, Paper W4E-2, doi: 10.1364/OFC.2015.W4E.2.

[93] H. Masuda, "Review of wideband hybrid amplifiers," in *Proc. Opt. Fiber Commun. Conf.*, 2000, pp. 2–4, doi: 10.1109/OFC.2000.868354.

[94] T. J. Xia *et al.*, "Transmission of 400G PM-16QAM channels over long-haul distance with commercial all-distributed Raman amplification system and aged standard SMF in field," in *Proc. Opt. Fiber Commun. Conf.*, 2014, pp. 1–3, Paper Tu2B.1, doi: 10.1364/OFC.2014.Tu2B.1.

[95] M. A. Iqbal, P. Harper, and W. Forysiak, "Improved design of ultra-wideband discrete Raman amplifier with low noise and high gain," in *Proc. Adv. Photon.*, 2018, Paper NpTh1H-2, doi: 10.1364/NP.2018.NpTh1H.2.

[96] U. C. De Moura *et al.*, "Multi–band programmable gain Raman amplifier," *J. Lightw. Technol.*, vol. 39,

no. 2, pp. 429–438, Oct. 26, 2020, doi: 10.1109/JLT.2020.3033768.
[97] L. E. Nelson, X. Zhou, B. Zhu, M. F. Yan, P. W. Wisk, and P. D. Magill, "All-Raman-amplified, 73 nm seamless band transmission of 9 Tb/s over 6000 km of fiber," *IEEE Photon. Technol. Lett.*, vol. 26, no. 3, pp. 242–245, Feb. 2014, doi: 10.1109/LPT.2013.2291399.
[98] C. Doerr *et al.*, "O, E, S, C, and L band silicon photonics coherent modulator/receiver," in *Proc. Opt. Fiber Commun. Conf.*, 2016, pp. 1–3, Paper Th5C.4, doi: 10.1364/OFC.2016.Th5C.
[99] C. Doerr and L. Chen, "Silicon photonics in optical coherent systems," *Proc. IEEE*, vol. 106, no. 12, pp. 2291–2301, Dec. 2018, doi: 10.1109/JPROC.2018.2866391.
[100] F. Hamaoka, "Ultra-wideband transmission and high-symbol rate signal handling technologies," in *Proc. Opt. Fiber Commun. Conf. (OFC)*, 2020, pp. 1–43, Paper W3E.1, doi: 10.1364/OFC.2020.W3E.1.
[101] W. Shi, Y. Tian, and A. Gervais, "Scaling capacity of fiber-optic transmission systems via silicon photonics," *Nanophotonics*, vol. 9, no. 16, pp. 4629–4663, Oct. 2020, doi: 10.1515/nanoph-2020-0309.
[102] M. Sena *et al.*, "Performance evaluation of InP-based DP-IQ modulators for multiband transmission systems," in *Proc. 22nd Int. Conf. Transp. Opt. Netw.*, 2020, pp. 1–4, Paper We.D2.5, doi: 10.1109/ICTON51198.2020.9203554.
[103] R. Halir *et al.*, "Ultra-broadband nanophotonic beamsplitter using an anisotropic sub-wavelength metamaterial," *Laser Photon. Rev.*, vol. 10, no. 6, pp. 1039–1046, Nov. 2016, doi: 10.1002/lpor.201600213.
[104] R. Emmerich *et al.*, "Enabling S-C-L-band systems with standard C-band modulator and coherent receiver using nonlinear predistortion," in *Proc. Opt. Fiber Commun. Conf. (OFC)*, 2021, pp. 1–3, Paper F4D.7.
[105] R. Elschner *et al.*, "Improving achievable information rates of 64-GBd PDM-64QAM by nonlinear transmitter predistortion," in *Proc. Opt. Fiber Commun. Conf.*, 2018, pp. 1–3, Paper M1C.2.
[106] M. Sena *et al.*, "An autonomous identification and pre-distortion scheme for cognitive transceivers using Bayesian optimization," in *Proc. 46th Eur. Conf. Opt. Commun.*, 2020, pp. 1–4, Paper Tu1D-7, doi: 10.1109/ECOC48923.2020.9333408.
[107] M. Sena *et al.*, "Bayesian optimization for nonlinear system identification and pre-distortion in cognitive transmitters," *J. Lightw. Technol.*, vol. 39, no. 15, pp. 5008–5020, Aug. 2021, doi: 10.1109/JLT.2021.3083676.
[108] M. Sena, R. Emmerich, B. Shariati, J. K. Fischer, and R. Freund, "Evaluation of an autonomous digital pre-distortion scheme for optical multiband systems," in *Proc. Opt. Fiber Commun. Conf.*, 2021, pp. 1–3, Paper F4D.5.
[109] P. W. Berenguer *et al.*, "Nonlinear digital pre-distortion of transmitter components," *J. Lightw. Technol.*, vol. 34, no. 8, pp. 1739–1745, Apr. 15, 2016, doi: 10.1109/JLT.2015.2510962.
[110] G. Khanna *et al.*, "A memory polynomial based digital pre-distorter for high power transmitter components," in *Proc. Opt. Fiber Commun. Conf.*, 2017, pp. 1–3, Paper M2C.4.
[111] S. J. B. Yoo, "Wavelength conversion technologies for WDM network applications," *J. Lightw. Technol.*, vol. 14, no. 6, pp. 955–966, Jun. 1996, doi: 10.1109/50.511595.
[112] K. Inoue, "Four-wave mixing in an optical fiber in the zero-dispersion wavelength region," *J. Lightw. Technol.*, vol. 10, no. 11, pp. 1553–1561, Nov. 1992, doi: 10.1109/50.184893.
[113] S. Watanabe, S. Takeda, and T. Chikama, "Interband wavelength conversion of 320 Gb/s (32×10 Gb/s) WDM signal using a polarization-insensitive fiber four-wave mixer," in *Proc. 24th Eur. Conf. Opt. Commun.*, vol. 3, 1998, pp. 83–87, doi: 10.1109/ECOC.1998.731208.
[114] T. Kato *et al.*, "Whole band wavelength conversion for wideband transmission," in *Proc. Opt. Fiber Commun. Conf. (OFC)*, 2021, pp. 1–3, Paper F1B.1.
[115] A. Shamsshooli *et al.*, "Emerging applications of wavelength conversion," in *Proc. IEEE Photon. Conf. (IPC)*, Oct. 2021, pp. 1–2, Paper ThE2.1, doi: 10.1109/IPC48725.2021.9592892.
[116] M. S. Sarwar, T. Sakamoto, T. Kato, and T. Hoshida, "TransLambda: A multi-band transmission system and its realization, practical applications and use cases in optical networks," in *Proc. Opt. Fiber Commun. Conf. (OFC)*, 2020, Paper M2G.6, doi: 10.1364/OFC.2020.M2G.6.
[117] H. Kawahara, M. Nakagawa, T. Seki, and T. Miyamura, "Experimental demonstration of wavelength-selective band/direction-switchable multi-band OXC using an inter-band all-optical wavelength converter," in *Proc. 46th Eur. Conf. Opt. Commun.*, 2020, p. 1–4, Paper Tu1H-5, doi: 10.1109/ECOC48923.2020.9333270.
[118] M.-C. Ho, K. Uesaka, M. Marhic, Y. Akasaka, and L. G. Kazovsky, "200-nm-bandwidth fiber optical amplifier combining parametric and Raman gain," *J. Lightw. Technol.*, vol. 19, no. 7, pp. 977–981, Jul. 2001, doi: 10.1109/50.933292.
[119] S. Takasaka, "Techniques for optical parametric amplification using highly nonlinear fiber," in *Proc. IEEE Photon. Conf. (IPC)*, Sep./Oct. 2019, pp. 1–2, Paper MC2.4, doi: 10.1109/IPCon.2019.8908421.
[120] T. Torounidis, P. A. Andrekson, and B. Olsson, "Fiber-optical parametric amplifier with 70-dB gain," *IEEE Photon. Technol. Lett.*, vol. 18, no. 10, pp. 1194–1196, May 15, 2006, doi: 10.1109/LPT.2006.874714.
[121] M.-C. Ho, M. E. Marhic, K. Y. K. Wong, and L. G. Kazovsky, "Narrow-linewidth idler generation in fiber four-wave mixing and parametric amplification by dithering two pumps in opposition of phase," *J. Lightw. Technol.*, vol. 20, no. 3, pp. 469–476, Mar. 2002, doi: 10.1109/50.988996.
[122] T. Kato *et al.*, "Fiber-optic frequency shifting of THz-range WDM signal using orthogonal pump-signal polarization configuration," in *Proc. Opt. Fiber Commun. Conf.*, 2018, pp. 1–3, Paper M3E.3, doi: 10.1364/OFC.2018.M3E.3.
[123] M. A. Foster, A. C. Turner, R. Salem, M. Lipson, and A. L. Gaeta, "Broad-band continuous-wave parametric wavelength conversion in silicon nanowaveguides," *Opt. Exp.*, vol. 15, no. 20, pp. 12949–12958, Oct. 2007, doi: 10.1364/OE.15.012949.
[124] C. J. Krückel *et al.*, "Continuous wave-pumped wavelength conversion in low-loss silicon nitride waveguides," *Opt. Lett.*, vol. 40, no. 6, pp. 875–878, Mar. 2015, doi: 10.1364/OL.40.000875.
[125] C. Lacava *et al.*, "Si-rich silicon nitride for nonlinear signal processing applications," *Sci. Rep.*, vol. 7, no. 1, pp. 1–3, Dec. 2017, doi: 10.1038/s41598-017-00062-6.
[126] R. F. Cregan *et al.*, "Single-mode photonic band gap guidance of light in air," *Science*, vol. 285, no. 5433, pp. 1537–1539, 1999, doi: 10.1126/science.285.5433.1537.
[127] P. Poggiolini and F. Poletti, "Opportunities and challenges for long-distance transmission in hollow-core fibres," *J. Lightw. Technol.*, vol. 40, no. 6, pp. 1605–1616, Mar. 15, 2022, doi: 10.1109/JLT.2021.3140114.
[128] A. Nespola *et al.*, "Ultra-long-haul WDM transmission in a reduced inter-modal interference NANF hollow-core fiber," in *Proc. Opt. Fiber Commun. Conf.*, 2021, pp. 1–3, Paper F3B.5.
[129] S. Ramachandran, "Measurement of multipath interference in the coherent crosstalk regime," *IEEE Photon. Technol. Lett.*, vol. 15, no. 8, pp. 1171–1173, Aug. 2003, doi: 10.1109/LPT.2003.814880.

ABOUT THE AUTHORS

Takeshi Hoshida (Senior Member, IEEE) received the B.E., M.E., and Ph.D. degrees in electronic engineering from The University of Tokyo, Tokyo, Japan, in 1993, 1995, and 1998, respectively.

Since he joined Fujitsu Laboratories Ltd., Kawasaki, Japan, in 1998, he has been engaged in the research and development of dense WDM optical transmission systems. From 2000 to 2002, he was with Fujitsu Network Communications, Inc., Richardson, TX, USA. Since 2007, he has been with Fujitsu Ltd., Kawasaki, Japan, and he currently heads Fujitsu's optical transmission research efforts.

Dr. Hoshida is a Senior Member of the Institute of Electronics, Information and Communication Engineers (IEICE) and a member of the Japan Society of Applied Physics (JSAP). He received the Commendation for Science and Technology by the Ministry of Education, Culture, Sports, Science and Technology (Awards for Science and Technology in Development Category) in 2020 and the Japan Patent Office Commissioner Award of the National Commendation for Invention in 2020.

Vittorio Curri (Senior Member, IEEE) received the Laurea degree in electrical engineering and the Scientific Doctoral degree in optical communications from the Politecnico di Torino (PoliTo), Turin, Italy, in 1995 and 1999, respectively.

He is currently a Founder Member of the OptCom Group and PhotonLab, PoliTo. He is also a Full Professor with the Department of Electronics and Telecommunications, PoliTo. He has been a Visiting Researcher with Stanford University, Stanford, CA, USA, and the University of California at Santa Barbara, Santa Barbara, CA, USA. He is one of the promoters of using the multiband transmission in single-mode fibers and investigates the topic within the H2020 ETN Wideband Optical Networks. He is also active in the analysis of the impact of physical layers on networking for planning and control of open and disaggregated optical networks, including AI techniques. He is also the Scientific Chair of the GNPy open source project within the consortium Telecom Infra Project. He is a coauthor of more than 330 scientific publications. His major research interests are in fiber transmission modeling, including nonlinearities, transmitter and receiver optimization, design strategies for optical links, Raman amplification, and simulation and modeling of optical communication systems.

Prof. Curri is an Optica Member.

Lidia Galdino (Senior Member, IEEE) received the M.Sc. and Ph.D. degrees in electronic and electrical engineering from the University of Campinas (UNICAMP), Campinas, Brazil, in 2008 and 2013, respectively.

From 2013 to 2022, she was with the Optical Networks Group, University College London (UCL), London, U.K., working as a Senior Research Associate until 2017. In 2018, she was appointed as a Lecturer and awarded a Royal Academy of Engineering Research Fellow at UCL on the topic of "Capacity-approaching, Ultra-Wideband Nonlinear Optical Fiber Transmission System." She is currently a System Engineering Manager at Corning Optical Fiber Communication, Ewloe, U.K. She is the author or coauthor of more than 100 scientific publications.

Dr. Galdino has been elected to the Board of Governors for the IEEE Photonics Society from 2020 to 2023. She was a corecipient of the RAEng Colin Campbell Mitchell Award in 2015 for pioneering contributions to optical communications technology and was named as one of the 2017 "Top 50 Women in Engineering under 35" by The Telegraph and Women in Engineering Society which features the U.K.'s top rising female stars of engineering. She has served on the Technical Program Committees for several conferences, including the European Conference on Optical Communication (ECOC) and the Optical Fiber Communication Conference (OFC). She is currently an Associate Editor of the *Journal of Lightwave Technology*.

David T. Neilson (Fellow, IEEE) received the B.Sc. and Ph.D. degrees in physics from Heriot-Watt University, Edinburgh, U.K., in 1990 and 1993, respectively.

He is currently the Group Leader for Optical Transmission Research with Nokia Bell Labs, Murray Hill, NJ, USA, where he is also a Bell Labs Fellow; the departments in the group conduct research into optical systems for terrestrial and undersea, including ultrahigh baud rates, modulation formats, and coding and the use of space-division multiplexing for scaling system capacities. He joined Nokia Bell Labs in 1998, where he led research on optical switching systems and optoelectronic integration; this includes micro electro mechanical system (MEMS) and liquid crystal on silicon (LCoS) for wavelength selective switches and optical cross-connects, and indium phosphide (InP) and silicon photonics. From 1993 to 1996, he was a Postdoctoral Researcher working on free-space optical interconnect and switching systems with Heriot-Watt University. From 1996 to 1998, he was a Visiting Scientist with NEC Research, Princeton, NJ, USA, researching optical interconnects for high-performance computing systems. He has authored more than 200 publications, patents, and short courses on both devices and systems in the field of optical interconnects and switching.

Dr. Neilson has served on and chaired several the IEEE Lasers and Electro-Optics Society (LEOS), the Optical Society of America (OSA), and the International society for optical and photonics, formerly Society of Photo-Optical Instrumentation Engineers (SPIE) conference programs in the field of optical interconnects and switching.

Wladek Forysiak (Member, IEEE) received the B.Sc. degree in physics from Imperial College London, London, U.K., in 1985, and the Ph.D. degree in physics from Heriot-Watt University, Edinburgh, U.K., in 1989.

He has a research background in nonlinear photonics, optical solitons, and high-speed optical fiber communication systems. In 2000, he co-founded Marconi-Solstis, Stratford-upon-Avon, U.K., and spent 15 years in wavelength-division multiplexing (WDM) system-related product development with Marconi, Coventry, U.K.; Ericsson, Coventry; and Oclaro, Paignton/Caswell, U.K. His current research interests include wideband optical fiber communication systems, optical devices, transceivers and subsystems, and the impact and mitigation of device and fiber nonlinearities.

Dr. Forysiak has served as a Royal Society Industry Fellow and an EPSRC Manufacturing Fellow. He is currently the EFFECT Photonics/Royal Academy of Engineering Research Chair in highly integrated coherent optical fiber communications.

Johannes K. Fischer (Senior Member, IEEE) received the Dipl.Ing. and Dr.Ing. degrees in electrical engineering from the Berlin Institute of Technology (TU Berlin), Berlin, Germany, in 2003 and 2009, respectively.

In 2010, he joined the Fraunhofer Institute for Telecommunications, Heinrich Hertz Institute, Berlin, where he is currently heading a research group on digital signal processing within the Department of Photonic Networks and Systems. He is the author or a coauthor of more than 120 articles and a book chapter. His research interests include advanced modulation formats, digital signal processing, and machine learning for optical systems.

Dr. Fischer is a member of the Verband der Elektrotechnik Elektronik Informationstechnik e.V. (VDE)„ where he also serves in the working group KT 3.1 "Modelling of Photonic Components and Systems" of the Information Technology Society. He has served on the Technical Program Committees of the OptoElectronics and Communications Conference (OECC) and the Optical Fiber Communication Conference (OFC).

Tomoyuki Kato (Member, IEEE) received the B.E., M.E., and Dr.Eng. degrees in electronic engineering from Yokohama National University, Yokohama, Japan, in 2001, 2003, and 2006, respectively.

From 2006 to 2009, he was a Research Associate with the Precision and Intelligence Laboratories, Tokyo Institute of Technology, Tokyo, Japan. Since he joined Fujitsu Laboratories Ltd., Kawasaki, Japan, in 2009, he has been engaged in the research of nonlinear optical signal processing for dense wavelength-division multiplexing optical transmission systems. Since 2019, he has been with Fujitsu Ltd.

Dr. Kato has served on the Technical Program Committees for the OptoElectronics and Communications Conference (OECC) and the European Conference on Optical Communication (ECOC).

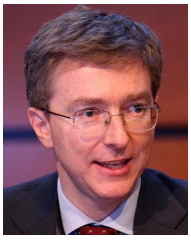

Pierluigi Poggiolini (Fellow, IEEE) received the M.S. *(cum laude)* and Ph.D. degrees from the Politecnico di Torino, Turin, Italy, in 1988 and 1993, respectively.

From 1990 to 1995, he was a Visiting Scholar and then a Postdoctoral Fellow with Stanford University, Stanford, CA, USA. Since 2010, he has been a Full Professor with the Politecnico di Torino. He was an elected member of the Academic Senate and the Board of Directors of the Politecnico di Torino from 2005 to 2010 and 2016 to 2020, respectively. He has published over 250 papers in leading journals and conferences. He is a coauthor of two papers that have received the Journal of Lightwave Technology Best Paper Award (published in 2011 and 2012). His current research interests include long-haul coherent transmission systems, nonlinear fiber effects, modeling and simulation of optical communications systems, and hollow-core fiber transmission systems.

Dr. Poggiolini is an OPTICA Fellow. He was the Technical Co-Chair of the European Conference on Optical Communication (ECOC) in 2010.